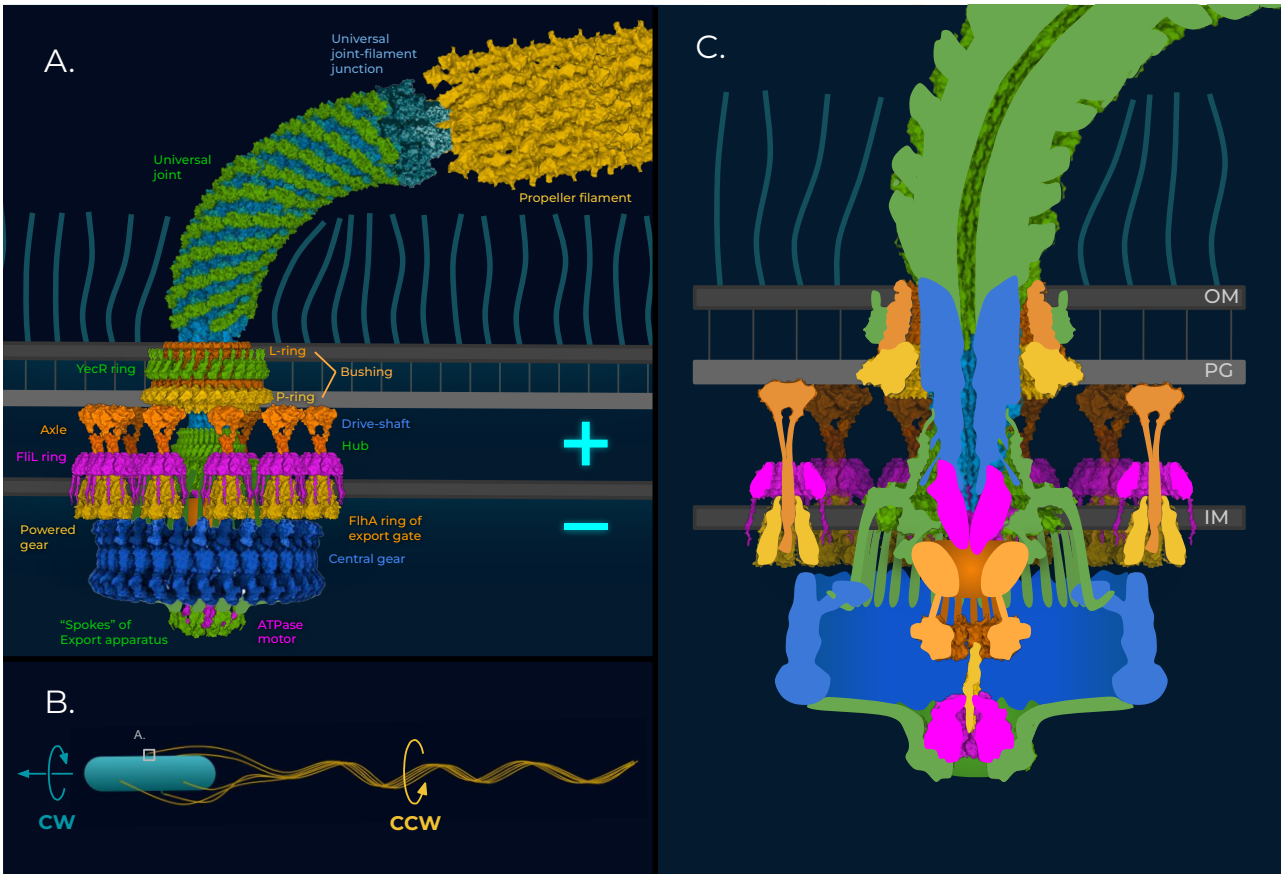

Figure 1. Bacterial flagellum of *E. coli*. (A) Representative illustration of *E. coli*'s flagellar motor, which is near identical to *Salmonella*'s flagellar motor. Illustration includes protein structures from *E. coli*, *Salmonella* and other species as well as Alphafold predictions[48, 49] when the structure in *E. coli* has not yet been solved experimentally. The + and - symbols indicate the relative charge difference across the inner membrane of the cell. Labels are colour-coordinated to label the component closest to each label of the same colour (apart from the universal joint which is coloured green and blue but has a green label). (B) Illustration of a swimming *E. coli* cell showing the coordinated rotation of the propeller filaments. The blue arrows indicate the movement of the cell body and the yellow arrow indicates the rotation of the flagella filaments. As well as propelling the cell forward, the CCW rotation of the filaments causes the cell to rotate CW. The square labeled A. indicates the location of the close up shown in A. (C) Illustrative cross-section of *E. coli*'s flagellar motor, coloured the same as in A (apart from the universal joint which is colored green). The export apparatus located inside the motor can clearly be seen in this cross-section (see figure 9). OM:Outer membrane; PG: Peptidoglycan layer (cell wall); IM: Inner membrane
Unless stated otherwise, protein structures in all figures are sourced from the RCSB protein data bank[50] or the Alphafold protein structure database.[48, 49] Protein graphics are made in part using Mol*.[51] The illustrations sometimes contain only parts of the cited PDB structures. The illustrations of the central gear in figures 1a, 2c, 3a, 6 and 7b is sourced from Carroll, *et al*[52] (used with permission. Image has been modified).
The illustration of the universal joint-filament junction in figures 1a, 2c and 21b is sourced from Green *et al*[38] (used with permission. Image has been modified).

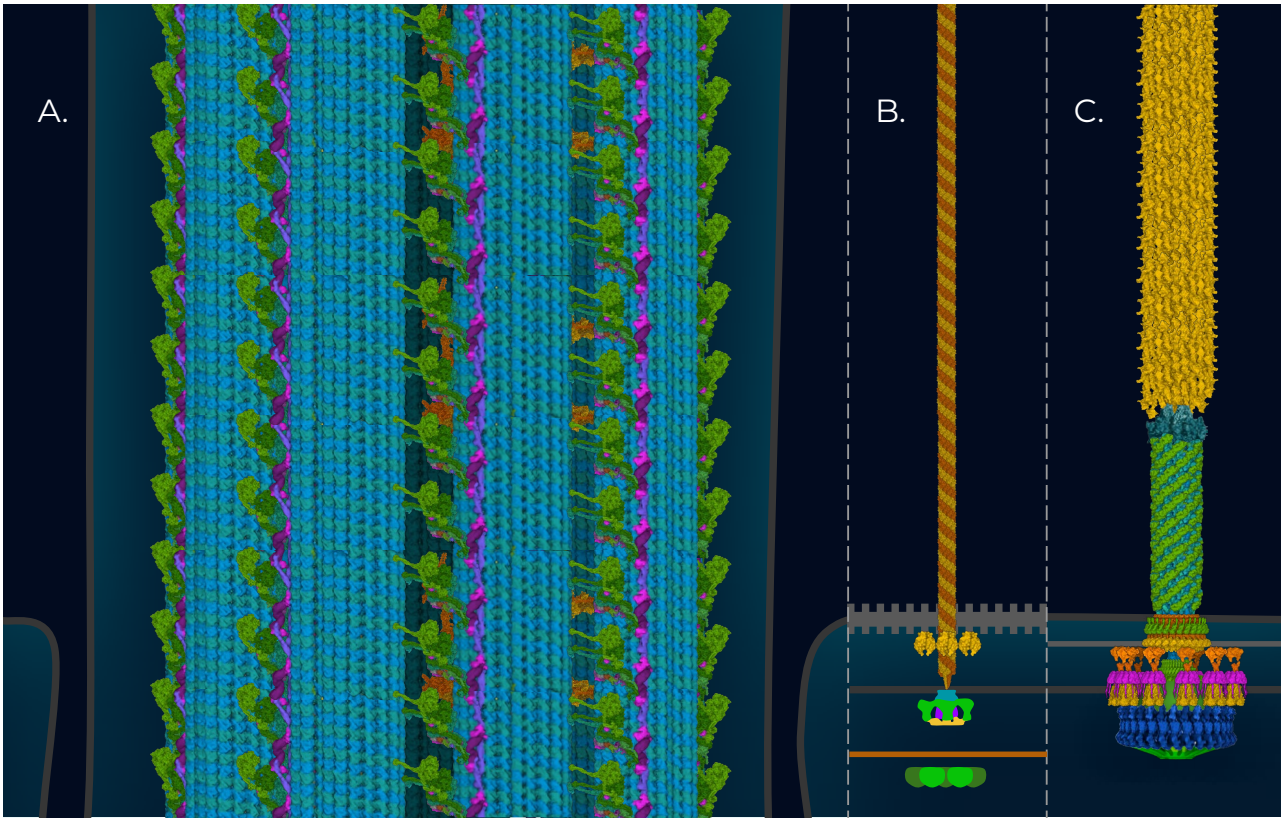

Figure 2. Comparison of flagella in eukarya (A), archaea (B) and bacteria (C). The universal joint of the bacterial flagellum is shown in a strait orientation for illustrative purposes and does not represent the wild-type structure of the universal joint. The archaeal flagellum is powered by ATP and has a propeller filament (PDB ID: 5TFY[53]) that is assembled from its base like a pilus, in contrast to bacterial flagella filaments which are assembled from the tip (PDB ID: 4ZBH[54] is show at archaellum base). The eukaryotic flagellum is by far the most complex, being made of over 400 different proteins that form an assembly of microtubules (shown in blue, PDB ID: 7RRO[55]), dynein (shown in green, PDB ID: 7K58[56]) and other components (shown in other colours, PDB ID: 7JTK[57]). Unlike archaeal and bacterial flagella, eukaryotic flagella do not rotate but sway side to side. See the caption of figure 1 for image credit for C.

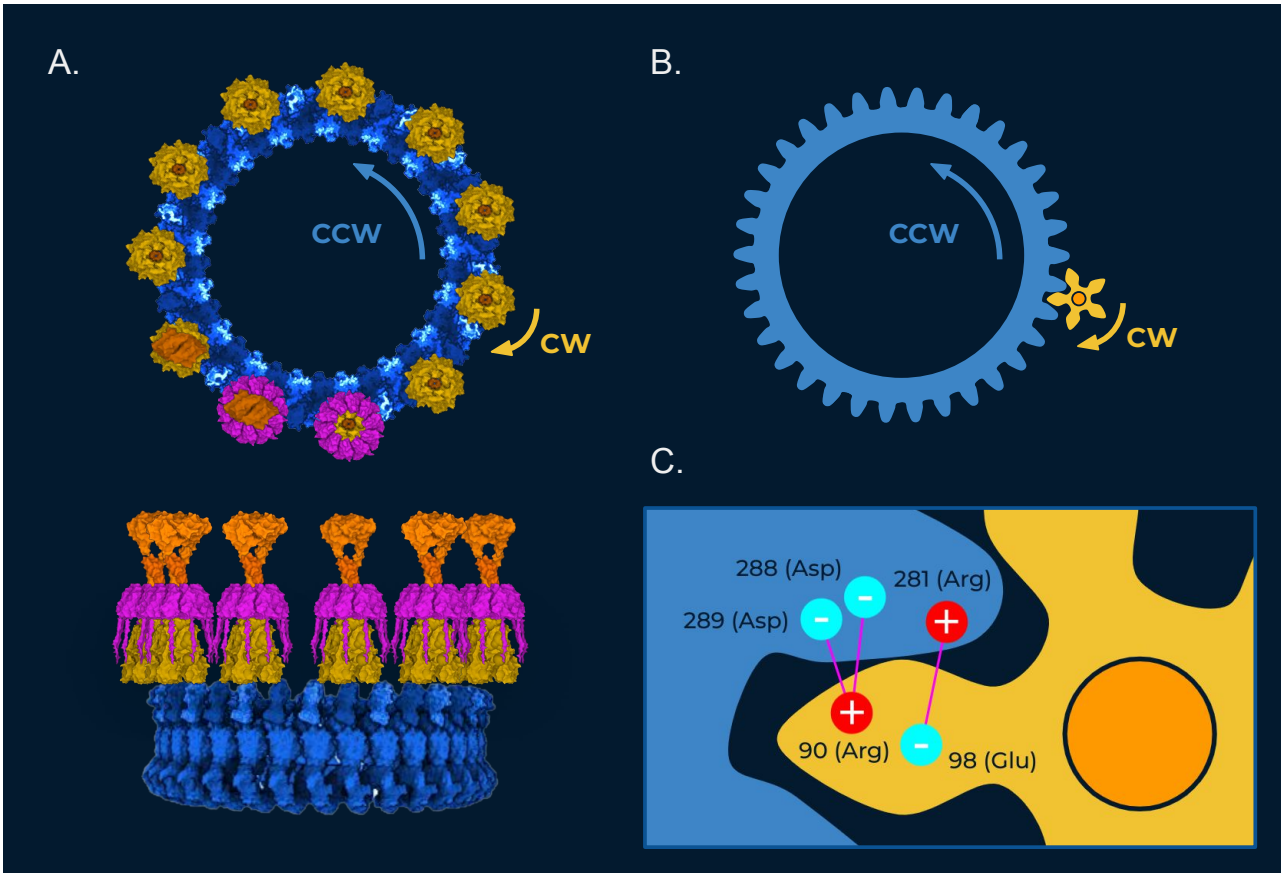

Figure 3. Representative illustration of the gearbox of the flagellar motor of *E. coli* and *Salmonella* in forward gear at full power. (A) Molecular surface representation of the gearbox viewed from the top (top) and side (bottom). In the top view, one MotA powered gear is shown with the cell-wall binding domain of MotB (shown in orange), one with the FliL ring (shown in purple) and one with both. The rest of the power gears are shown only with the axle domain of MotB (shown in orange). See the caption of figure 1 for image credit. (B) Diagram of a two-cogwheel system with a gear ratio of 34:5. (C) Residues involved in electrostatic interactions between the central gear and powered gears. Residue numbers correspond to sequences in *E. coli*. It is possible that the gear teeth are not in an interlocking orientation but are oriented with the gear teeth of the power gear positioned directly above the gear teeth of the central gear.

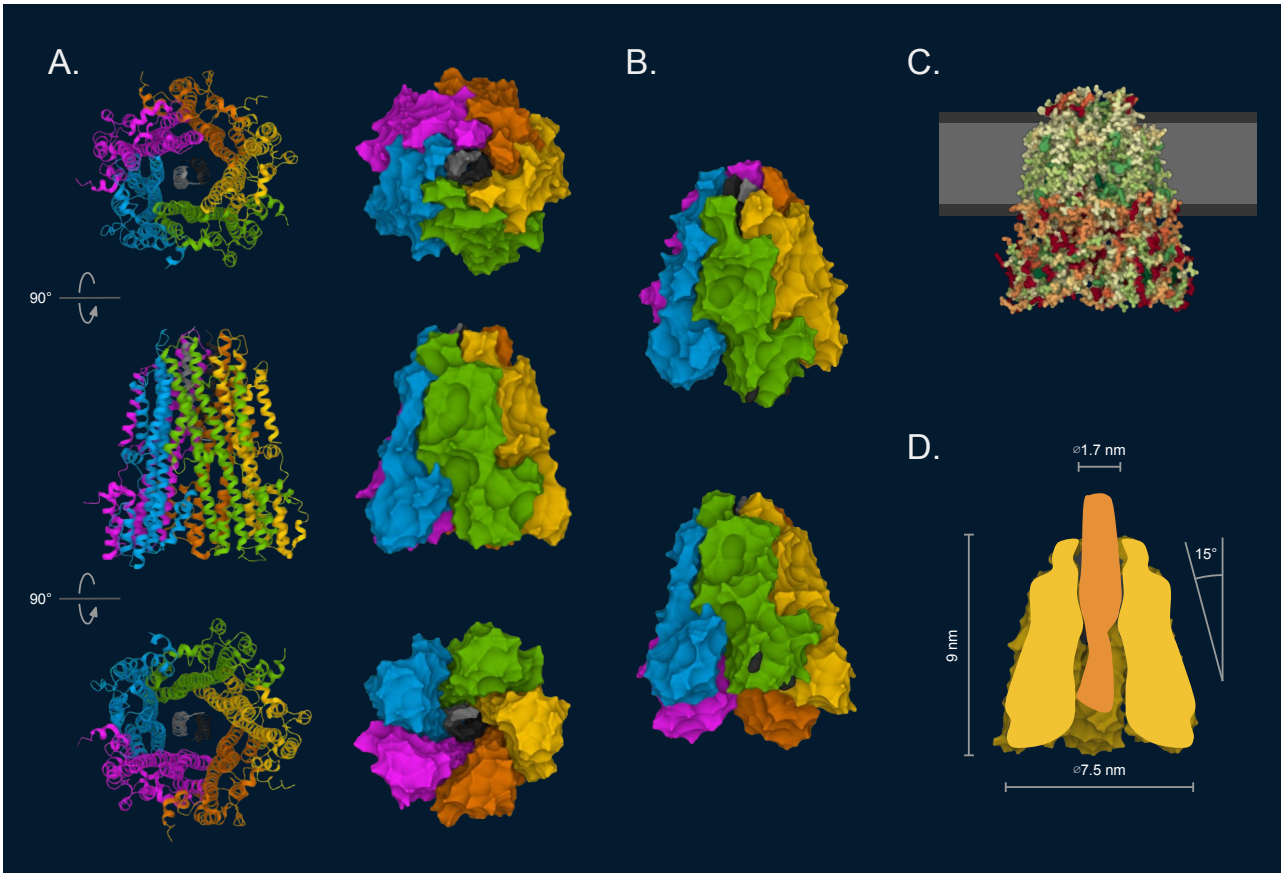

Figure 4. The MotA powered gear of *Bacillus subtilis* (PDB ID: 6YSL[13]), which is expected to be very similar to that in *E. coli* and *Salmonella*. (A) The ribbon diagram (left) and molecular surface representation (right) of the MotA powered gear. The MotB axle is shown in light and dark gray. (B) Isometric views of MotA powered gear. Residues that form electrostatic interactions with the central gear (90 and 98 in *B. subtilis*) have been coloured dark gray on the green MotA subunit (C) Hydrophobicity of residues (red= hydrophilic; green = hydrophobic). The approximate position of the hydrophilic and hydrophobic portions of the cytoplasmic membrane have been shown in dark gray and light gray, respectively. (D) Illustrative cross-section of MotA powered gear (yellow) and MotB axle (orange).

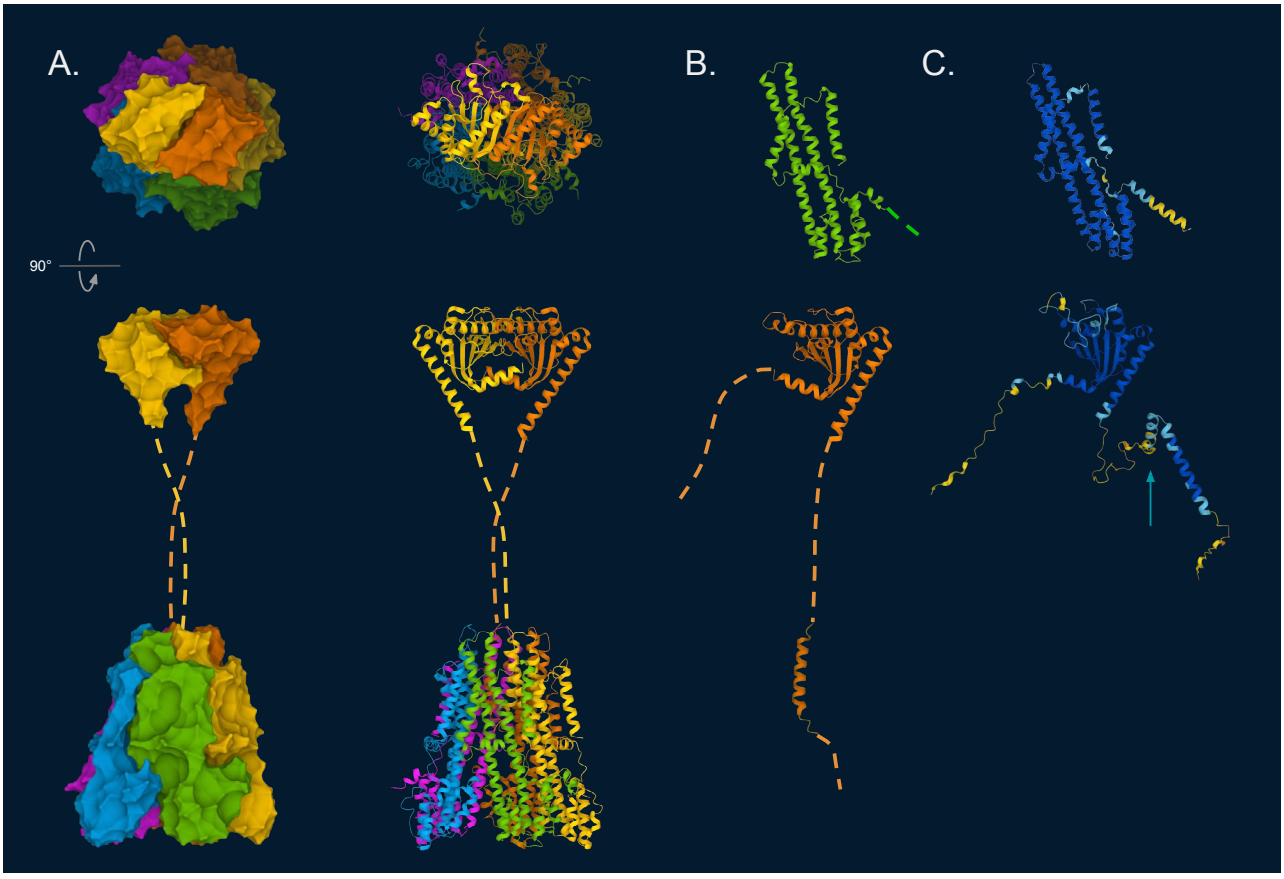

Figure 5. The MotAB complex of *Bacillus subtilis*. (A) The molecular surface representation (left) and ribbon diagram (right) of the MotAB complex. MotA subunits (PDB ID: 6YSL) shown in blue, green, yellow, orange and purple, respectively. MotB subunits (PDB IDs: 2ZVY[58] & 6YSL) shown in yellow and orange, respectively. (B) The solved structure of MotA (upper) and MotB (lower). The dashed lines indicate portions of the structures that have not been solved experimentally and are likely unstructured (apart from the plug region) (C) The Alphafold prediction of MotA (upper, P28611) and MotB (lower, P0AF07), showing portions of proteins not yet solved (dark blue = very high confidence in prediction accuracy, orange = very low confidence). The blue arrow points to the plug region of MotB.

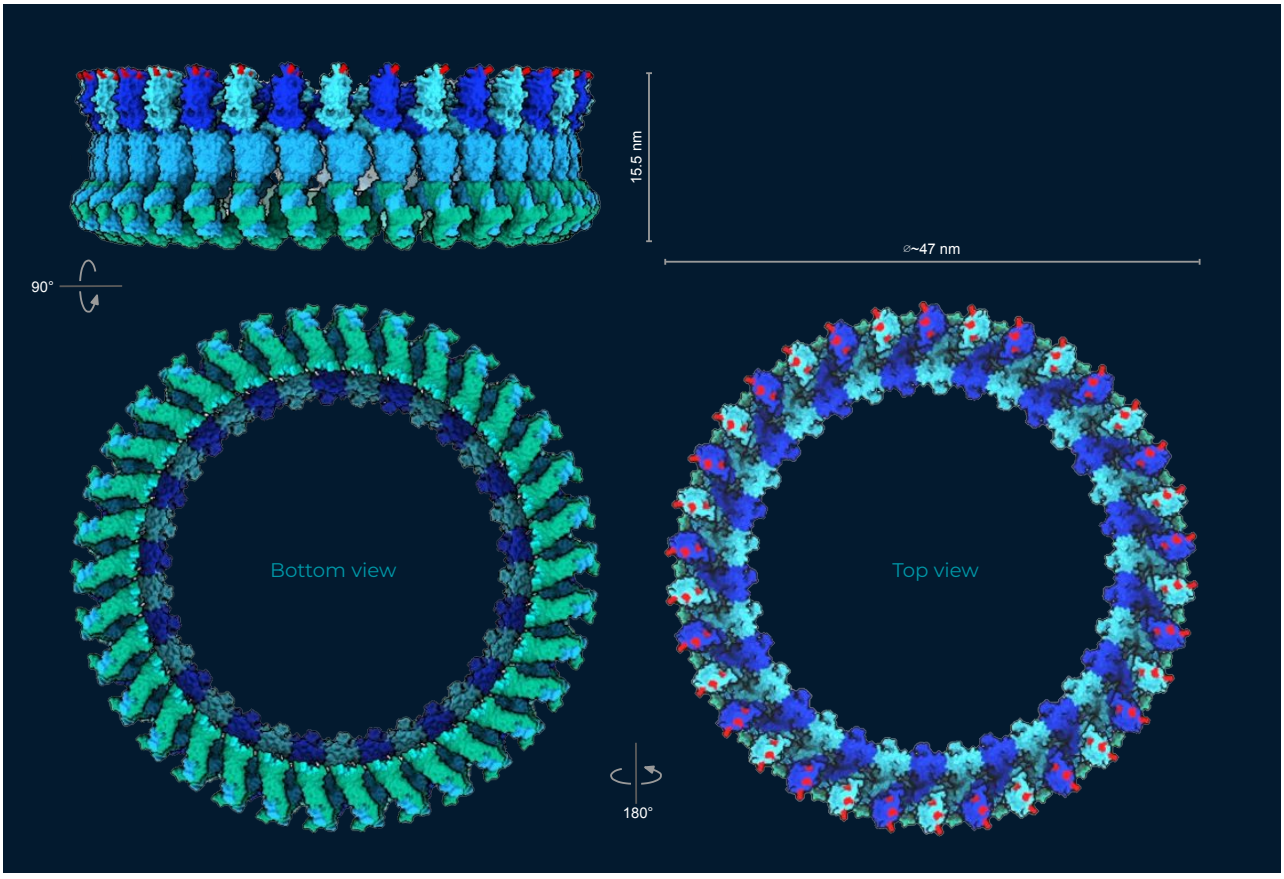

Figure 6. Orthographic projection of the predicted structure of the central gear (C-ring) of *Vibrio alginolyticus* which is believed to have a very similar structure to the central gear of *E. coli* and *Salmonella*. FliG is shown in dark blue and cyan, FliM is shown in light blue, and FliN is shown in green. FliG residues which form electrostatic interactions with MotA are shown in red. See the caption of figure 1 for image credit.

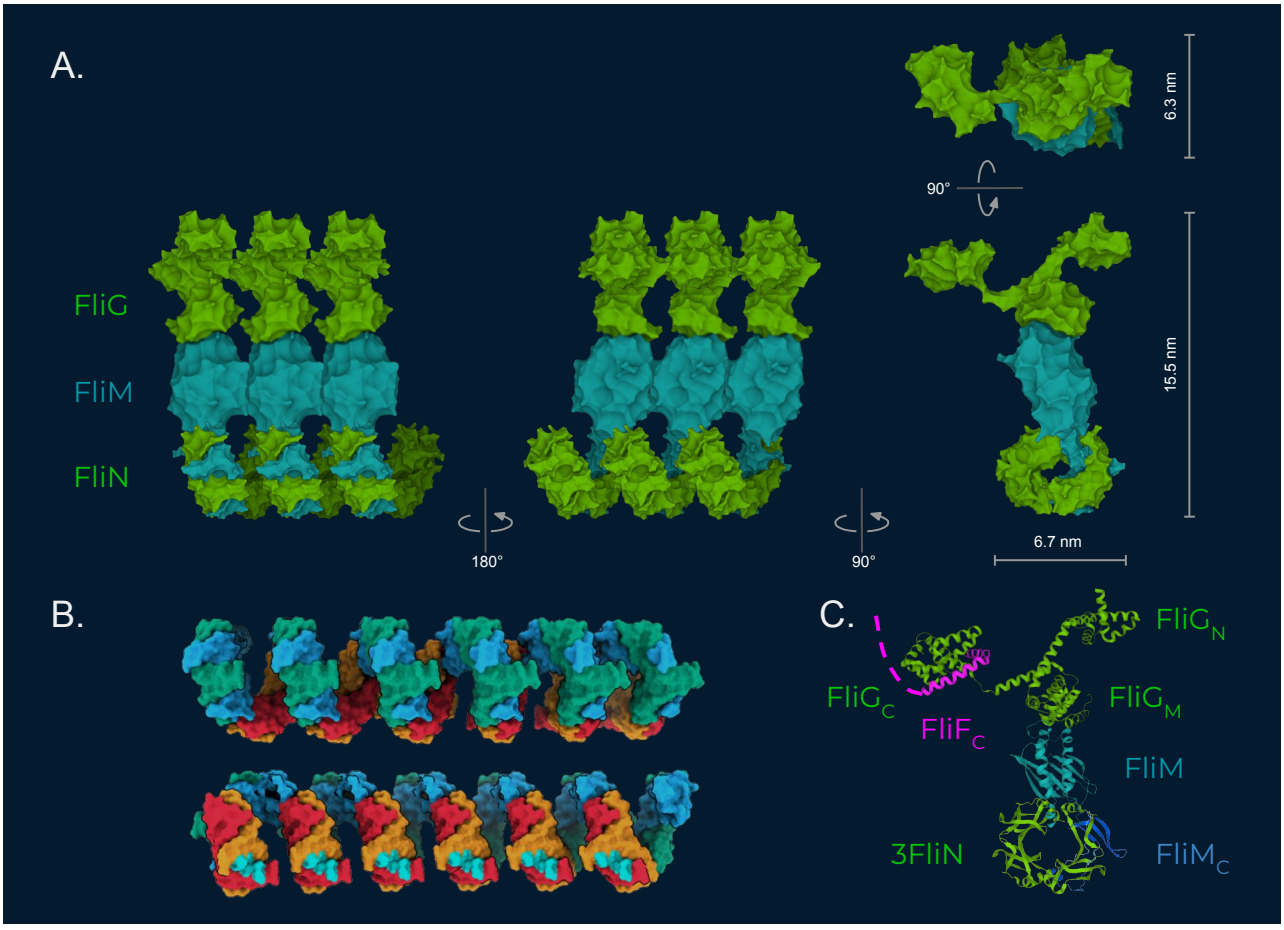

Figure 7. The repeating unit of the central gear (C-ring). (A) Molecular surface representation of the repeating unit of the central gear. Three repeating units are shown on the left two images while only one is shown in the right two. This model has been made by combining the following PDB files: 3HJL,[i] 4QRM,[ii] and 5XRW.[iii] The spiral structure at the base is made of repeating units of FliN and FliMc. The structure of the C-terminal of FliM is not known but is believed to be very similar to the structure of FliN and so a FliN subunit has been used to illustrate FliMc. (B) Close up of the spiral structure at the base of the central gear, viewed from outside the central gear (top) and inside the central gear (bottom). FliN subunits are shown in red, orange and green. FliMc is shown in blue. A hydrophobic patch, where the export apparatus attaches, is shown in cyan in the lower image. See the caption of figure 1 for image credit. (C) Cartoon representation of the predicted structure of one repeating unit of the central gear. The N-terminal, middle terminal and C-terminal of FliG are labeled FliG$_N$, FliG$_M$, and FliG$_C$, respectively. The C-terminal of FliF is shown in purple. This model has been made by combining the following PDB files: 3HJL, 5WUJ,[iv] 4QRM, and 5XRW. The Alphafold prediction of the C-terminal of FliM (P06974) has been used (coloured according to prediction confidence level) since its structure has not yet been solved experimentally.

i) Lee, L.K., Ginsburg, M.A., Crovace, C., Donohoe, M., and Stock, D., Structure of the torque ring of the flagellar motor and the molecular basis for rotational switching, Nature **466**:996–1000, 2010.
ii) Sircar, R., Borbat, P.P., Lynch, M.J., Bhatnagar, J., Beyersdorf, M.S., Halkides, C.J., Freed, J.H., and Crane, B.R., Assembly states of FliM and FliG within the flagellar switch complex, *J. Mol. Biol.* **427**:867–886, 2015.
iii) Lam, K.H., Xue, C., Sun, K., Zhang, H., Lam, W., Zhu, Z., Ng, J., Sause, W.E., Lertsethtakarn, P., Lau, K.F., Ottemann, K.M., and Au, S., Three SpoA-domain proteins interact in the creation of the flagellar type III secretion system in *Helicobacter pylori*, *J. Biol. Chem.* **293**:13961–13973, 2018.
iv) Xue, C., Lam, K. H., Zhang, H., Sun, K., Lee, S. H., Chen, X., and Au, S., Crystal structure of the FliF-FliG complex from *Helicobacter pylori* yields insight into the assembly of the motor MS-C ring in the bacterial flagellum, *J. Biol. Chem.* **293**:2066–2078, 2018.

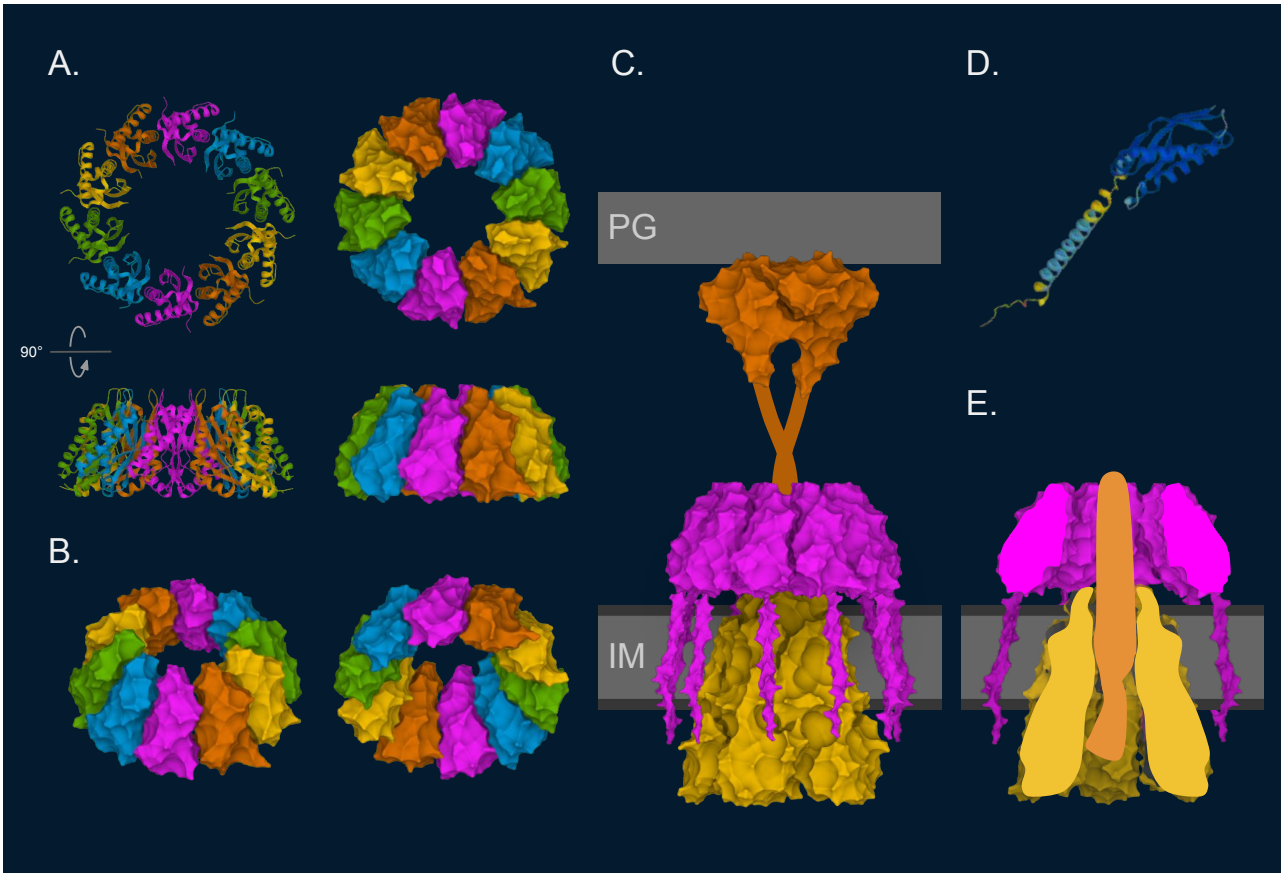

Figure 8. The FliL decameric ring of *Vibrio alginolyticus* which likely has a very similar structure of the central gear of *E. coli* and *Salmonella*. (A) Ribbon diagram (left) and molecular surface representation (right) of FliL decameric ring (PDB ID: 6AHQ[i]). (B) Isometric views of FliL decameric ring (C) FliL-MotAB complex, using PDB files from *Salmonella* (2ZVY), *Bacillus subtilis* (6YSL) and *Vibrio alginolyticus* (6AHQ). The Alphafold prediction of the transmembrane portion of FliL from *E. coli* (K-12, P0ABX8) has been added to the model. The transmembrane portions give the ring a jellyfish-like appearance. PG: Peptidoglycan cell wall; IM: Inner membrane. (D) Alphafold prediction of FliL from *E. coli* (K-12, P0ABX8). (E) Cross-section of FliL-MotAB complex.

i) Takekawa, N., Isumi, M., Terashima, H., Zhu, S., Nishino, Y., Sakuma, M., Kojima, S., Homma, M., and Imada, K., Structure of *Vibrio* FliL, a New stomatin-like protein that assists the bacterial flagellar motor function, *mBio* **10**(2):e00292–19, 19 Mar 2019.

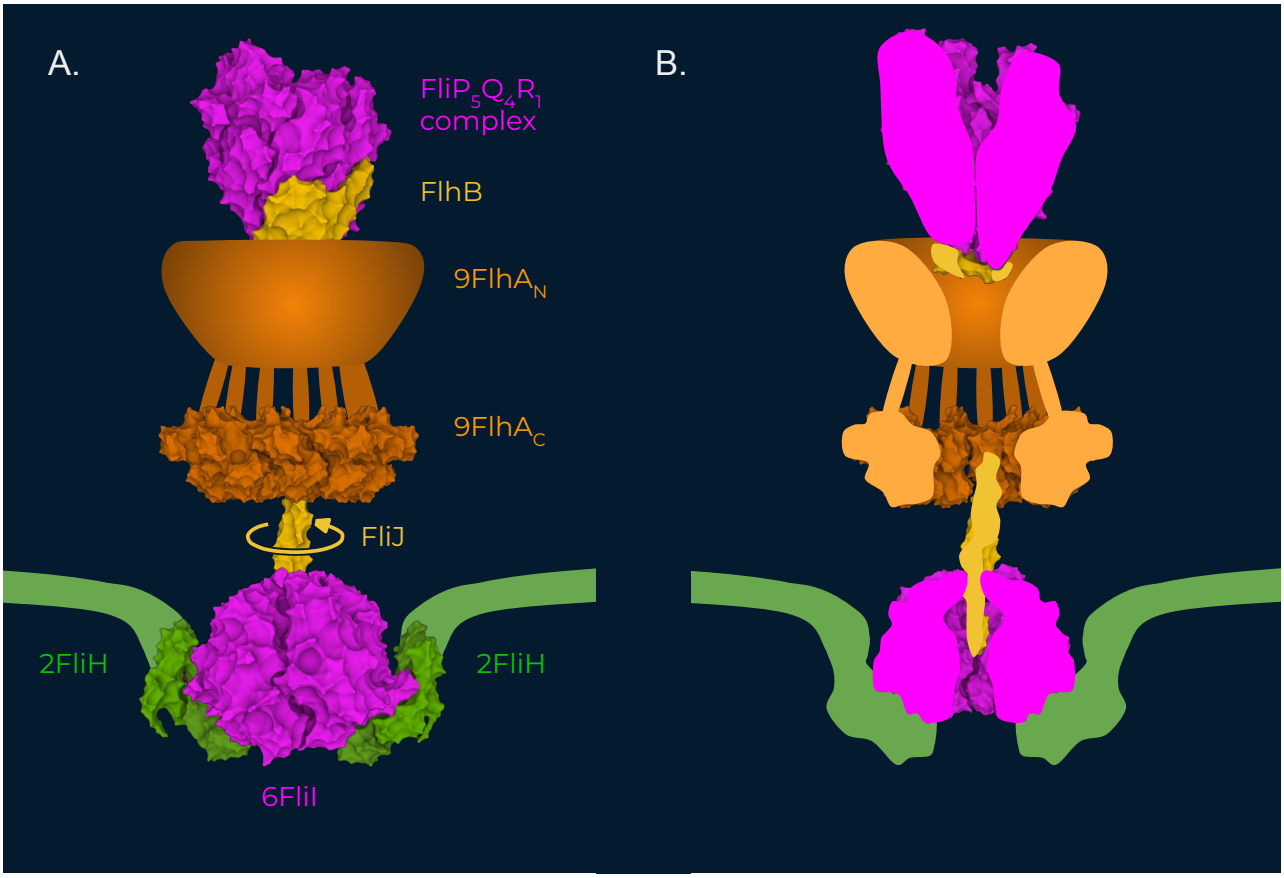

Figure 9. The flagella-specific export apparatus (PDB IDs: 6S3L,[i] 7AMY,[ii] 6NJO (homologous complex used in place of FliI to represent FliI),[iii] 3AJW,[iv] and 5B0O[v]). (A) Molecular surface representation of the export gate (made of the FliPQR complex, FlhB, and FlhA), flagella-specific ATPase motor (made of FliJ, and FliI), and spoke structure (made of FliH). Labels are colour coordinated to label the component closest to them of the same colour. The atomic structure of the upper portion of FlhA has not yet been solved. Proteins which form the axial components are exported through the inner channel of the FliPQR complex, when opened, for delivery to their associated assembly sites. The yellow arrow indicates the rotation of the FliJ shaft of the ATPase motor. (B) Cross-section of the export apparatus, coloured the same as in A.

i) Kuhlen, L., Johnson, S., Zeitler, A., Bäurle, S., Deme, J.C., Caesar, J.J.E., Debo, R., Fisher, J., Wagner, S., and Lea, S.M., The substrate specificity switch FlhB assembles onto the export gate to regulate type three secretion, *Nature Commun.* **11**(1):1296, 10 Mar 2020.
ii) Kuhlen, L., Johnson, S., Cao, J., Deme, J.C., and Lea, S.M., Nonameric structures of the cytoplasmic domain of FlhA and SctV in the context of the full-length protein, *PloS One* **16**(6), e0252800, 18 Jun 2021.
iii) Majewski, D.D., Worrall, L.J., Hong, C., Atkinson, C.E., Vuckovic, M., Watanabe, N., Yu, Z., and Strynadka, N.C.J., Cryo-EM structure of the homohexameric T3SS ATPase-central stalk complex reveals rotary ATPase-like asymmetry, *Nature Commun.* **10**(1):626, 7 Feb 2019.
iv) Ibuki, T., Imada, K., Minamino, T., Kato, T., Miyata, T., and Namba, K., Common architecture of the flagellar type III protein export apparatus and F- and V-type ATPases, *Nature Structural and Mol. Biol.***18**(3), 277–282, 30 Jan 2011.
v) Imada, K., Minamino, T., Uchida, Y., Kinoshita, M., and Namba, K., Insight into the flagella type III export revealed by the complex structure of the type III ATPase and its regulator, PNAS **113**(13):3633–3638, 16 Mar 2016.

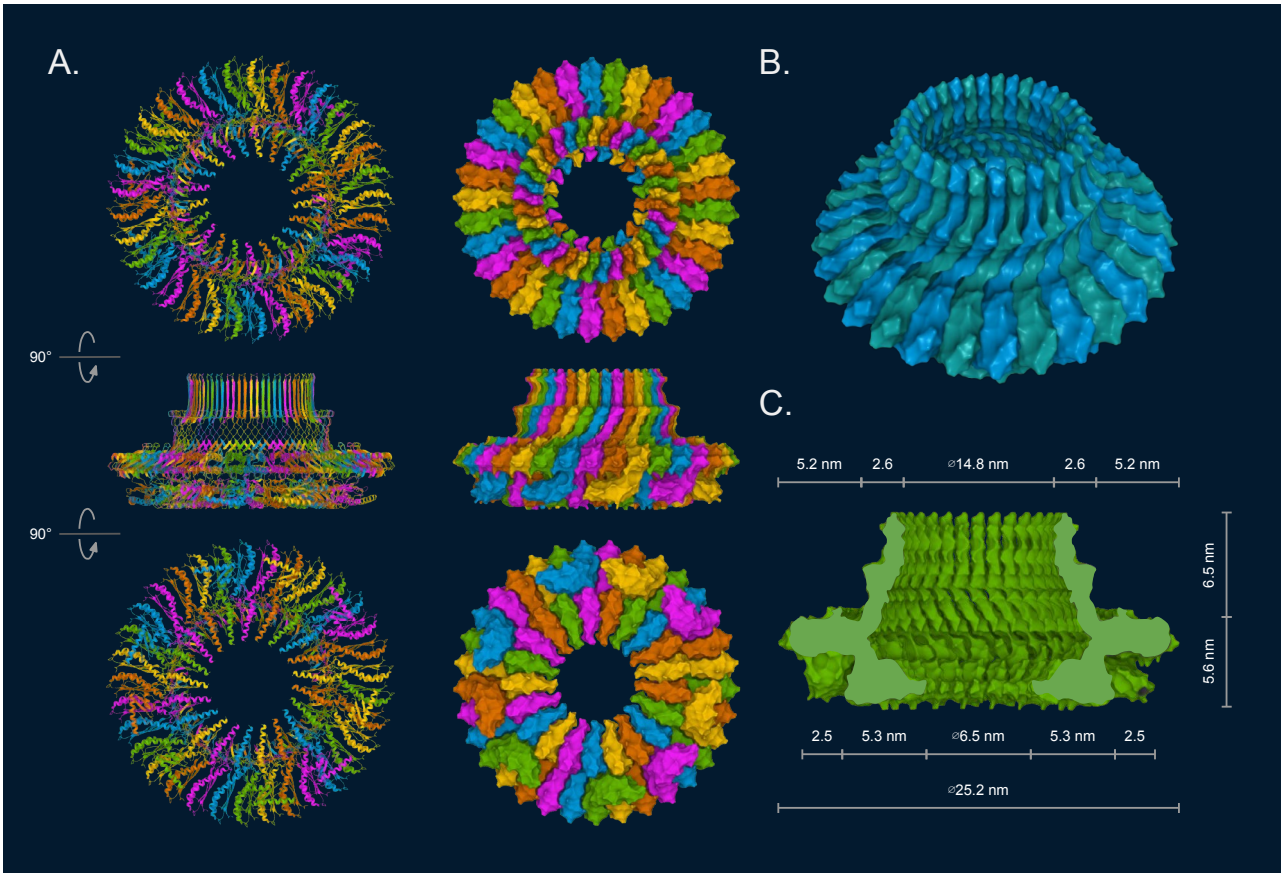

Figure 10. The hub (MS-ring) of *Salmonella*. (A) Ribbon diagram (left) and molecular surface representation (right) of the hub (PDB ID: 6SCN[i]). The ribbon diagram shows the beautifully elegant design of the hub's socket. (B) 3-dimensional view of the hub. (C) Cross-section of the hub, showing the inner cavity which houses the FliPQR complex and proximal driveshaft. This cavity becomes narrower at the top to prevent the FliPQR complex and driveshaft from slipping out of the hub socket.

i) Tan, J., Zhang, X., Wang, X., Xu, C., Chang, S., Wu, H., Wang, T., Liang, H., Gao, H., Zhou, Y., and Zhu, Y., Structural basis of assembly and torque transmission of the bacterial flagellar motor, *Cell* **184**:2665–2679, 2021.

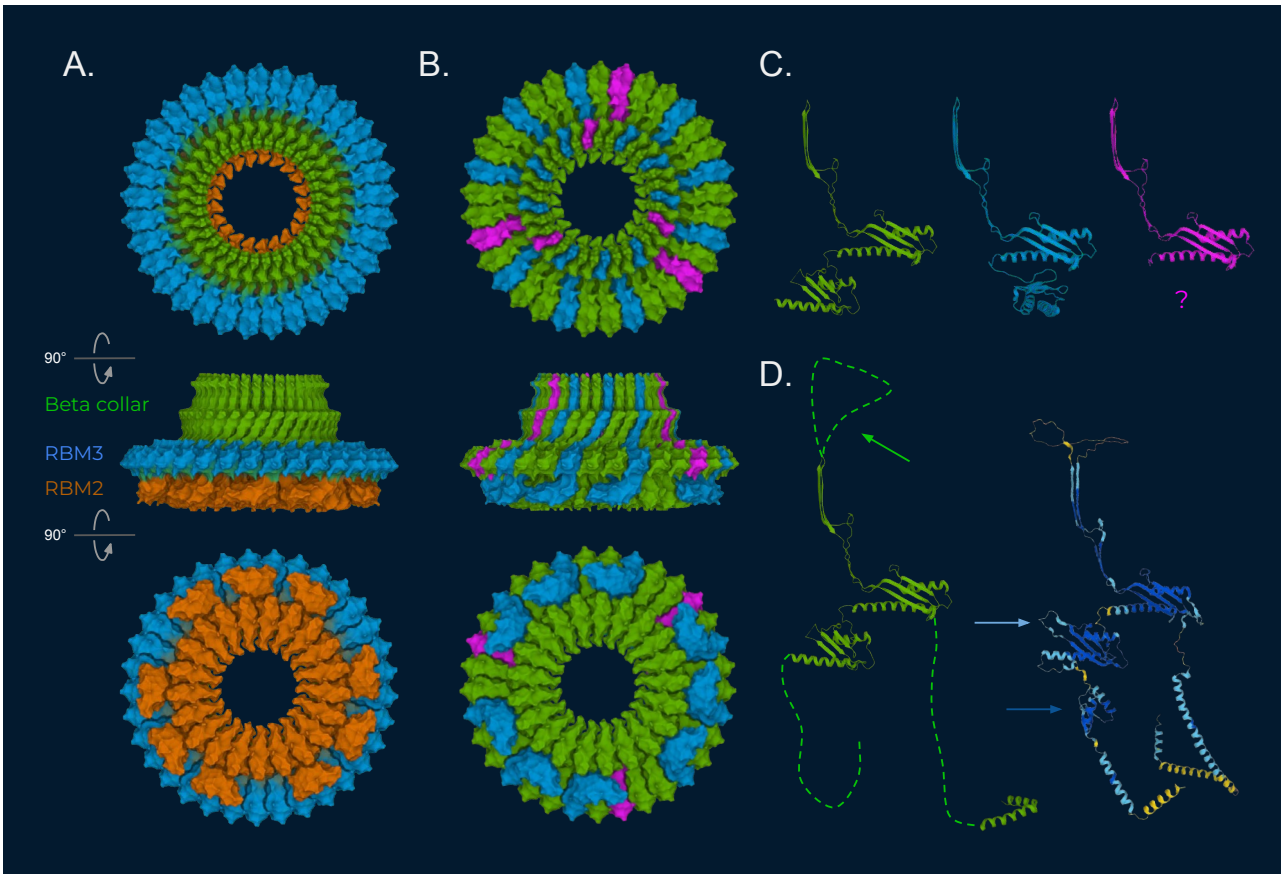

Figure 11: The hub (MS-ring) of *Salmonella* with 33 subunits (PDB ID: 6SCN). (A) Molecular surface representation of the domains of FliF: RBM2 (orange), RBM3 (blue), beta collar (green). RBM1, a portion above the beta collar, and the N- and C- terminals are not shown (see D). (B) The FliF subunits in the hub fold into three distinct conformations, shown here in green, blue and purple, respectively. The subunits shown here in green also have slightly different conformations as the relative position of the inner ring domain (RBM2) to the outer ring domain (RBM3) is different depending on their position around the hub. The RBM2 domains of the pink subunits are not shown. (C) Ribbon diagrams of the three distinct fold confirmations shown in B. The location of the RBM2 domain in the subunit coloured purple is not known. (D) The solved structure (left, PDB IDs: 6SCN and 5WUJ) and the Alphafold prediction (right, P25798, coloured according to prediction confidence) of FliF. The green arrow points to the portion of FliF which contains the L1 and L2 segments which bind to the proximal driveshaft. The light blue arrow points to a loop structure which extends from the RBM2 domain and contacts the FliPQR complex. The dark blue arrow points to the RBM1 domain.

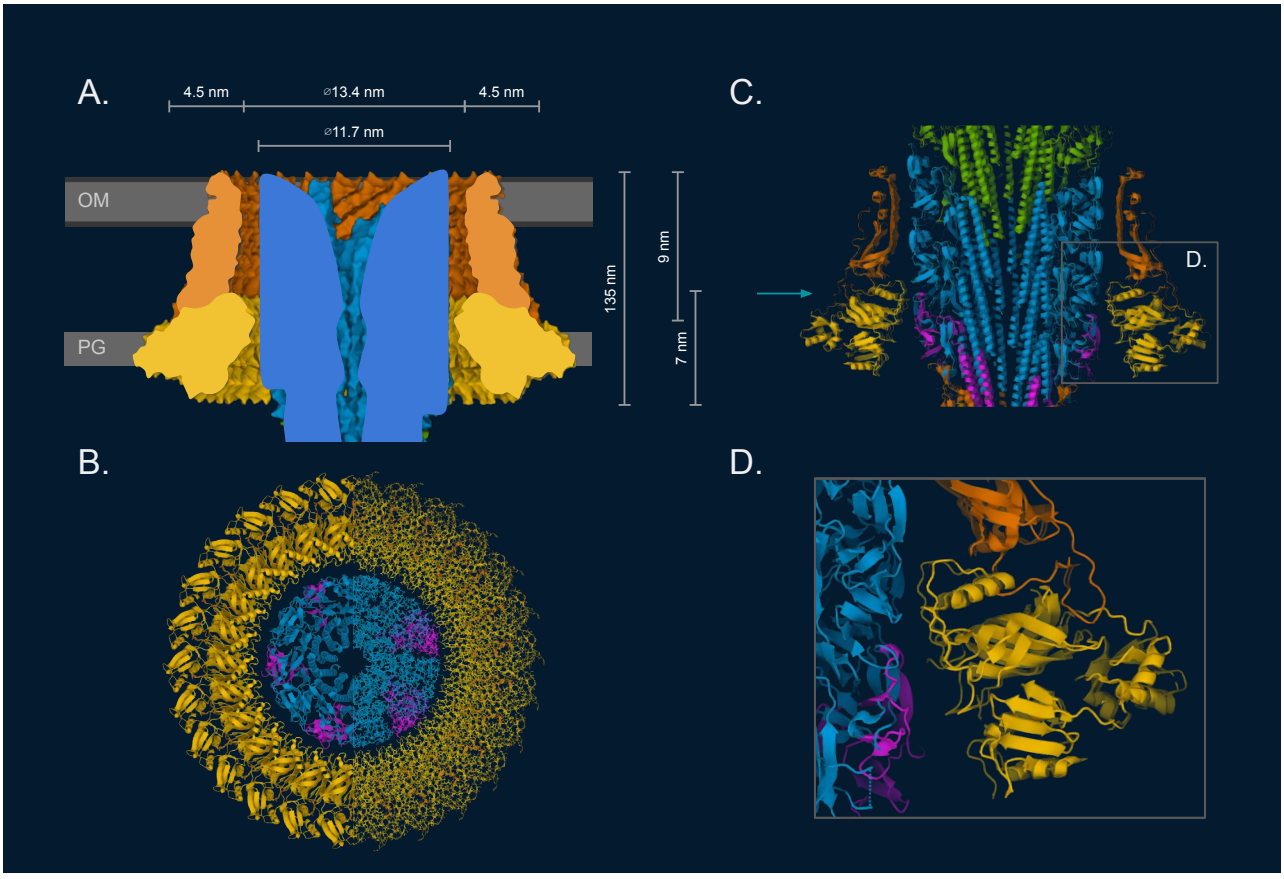

Figure 12. Interactions between the driveshaft and bushing. (A) Vertical cross-section of the driveshaft inside the bushing. The driveshaft is shown in blue, the L-ring in orange and the P-ring in yellow. OM: outer membrane; PG: peptidoglycan layer (cell wall). (B) Horizontal cross-section through the driveshaft and bushing at the point of closest contact between them as indicated with the blue arrow in C. The left half is a ribbon diagram representation while the right half is a ball-and-stick representation. It is especially clear in the ball-and-stick representation that the driveshaft is just the right diameter to slot through the hole inside the bushing and is almost perfectly round so that it can rotate with little friction. (C) Vertical cross-section through a ribbon diagram representation of the driveshaft (blue, purple and orange), bushing (orange and yellow) and part of the universal joint (green). Blue arrow points to the vertical position of knife-edge seal of the bushing around the driveshaft. (D) Close up as indicated with the box in C.

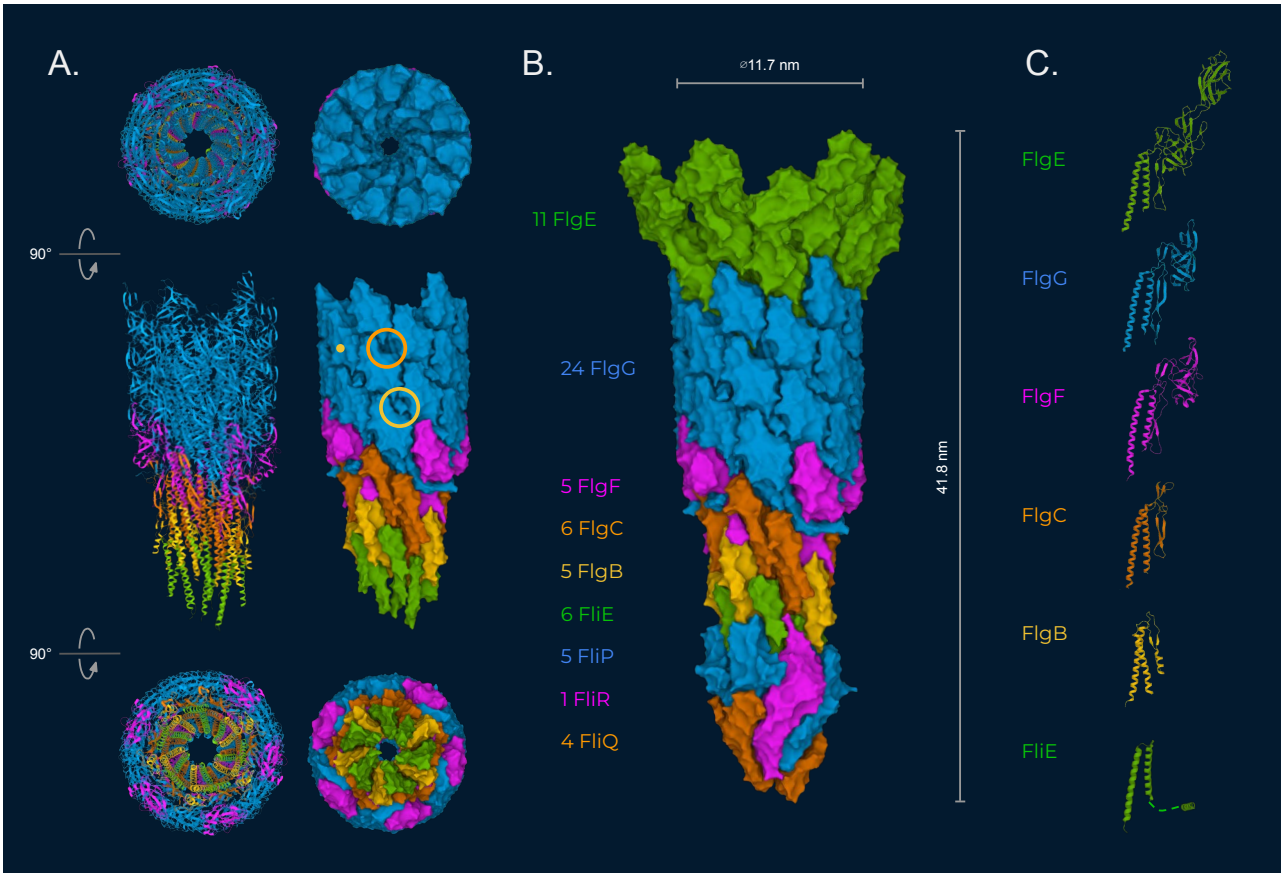

Figure 13. Driveshaft (rod) of *Salmonella* (PDB ID: 7E80[i]). (A) Ribbon diagram (left) and molecular surface representation (right) of the driveshaft. The orange circle shows an empty hole between FlgG subunits which causes more flexibility in the upper part of the distal driveshaft. The yellow circle shows a hole which is filled with the GSS region of the FlgG subunit marked with the yellow dot. This provides rigidity and stability to the lower distal driveshaft. (B) Molecular surface representation of the driveshaft with the FliPQR complex at bottom and 11 subunits of the universal joint at the top. The intricate interlocking of each of these proteins can clearly be seen. The GSS region of the Dc domain of the blue FlgG subunit in the centre of the image can been seen hooking under a purple FlgF subunit to lock the structure together. (C) Ribbon diagrams of the solved structures of the universal joint (FlgE) and driveshaft (FlgG, FlgF, FlgC, FlgB, FliE) subunits. Sections of some subunits have not yet been solved. The structure of FliE is from PDB ID: 7CGO. The structures of the remainder are from PDB ID: 7E80.

i) Tan, J., Zhang, X., Wang, X., Xu, C., Chang, S., Wu, H., Wang, T., Liang, H., Gao, H., Zhou, Y., and Zhu, Y., Structural basis of assembly and torque transmission of the bacterial flagellar motor, *Cell* **184**:2665–2679, 2021.

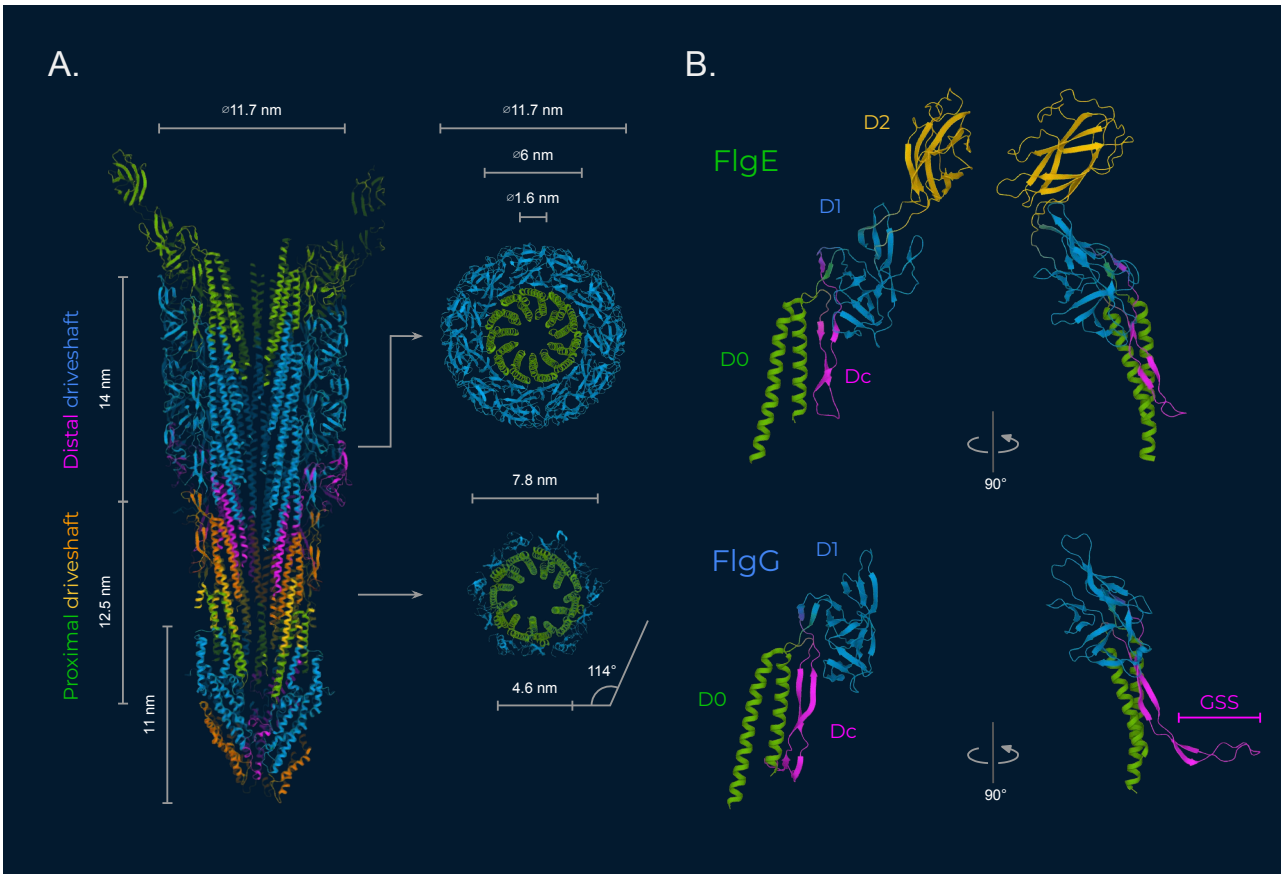

Figure 14. Driveshaft (rod) of *Salmonella*. (A) Vertical (left) and horizontal (right, viewed from below) cross-sections through a ribbon diagram representation of the structure in figure 13b. In the vertical cross-section, subunits have been coloured the same as it figure 13b. In the horizontal cross-sections, the inner and outer layers of the driveshaft are shown in green and blue, respectively. The inner channel of the driveshaft can be clearly seen in all slices. The driveshaft subunits assemble into a helix with approximately 5.5 subunits per turn in the 1-start direction resulting in a cross-section shape that is midway between a pentagon and a hexagon as seen in the lower horizontal cross-section. In the distal driveshaft this shape is changed to a near-perfect circle, as seen in the upper horizontal cross-section, which is needed for smooth rotation inside the bushing. Arrows indicate approximate height of each horizontal cross-section. (B) Comparison of the structure of the universal joint subunit FlgE (top, PDB ID: 7E80) and the distal driveshaft subunit FlgG (bottom, PDB ID: 7E80), showing their respective domains. The location of the GSS region in FlgG, which is absent in FlgE, is labelled bottom right. The absence of this region in FlgE makes the upper distal driveshaft and universal joint more flexible.

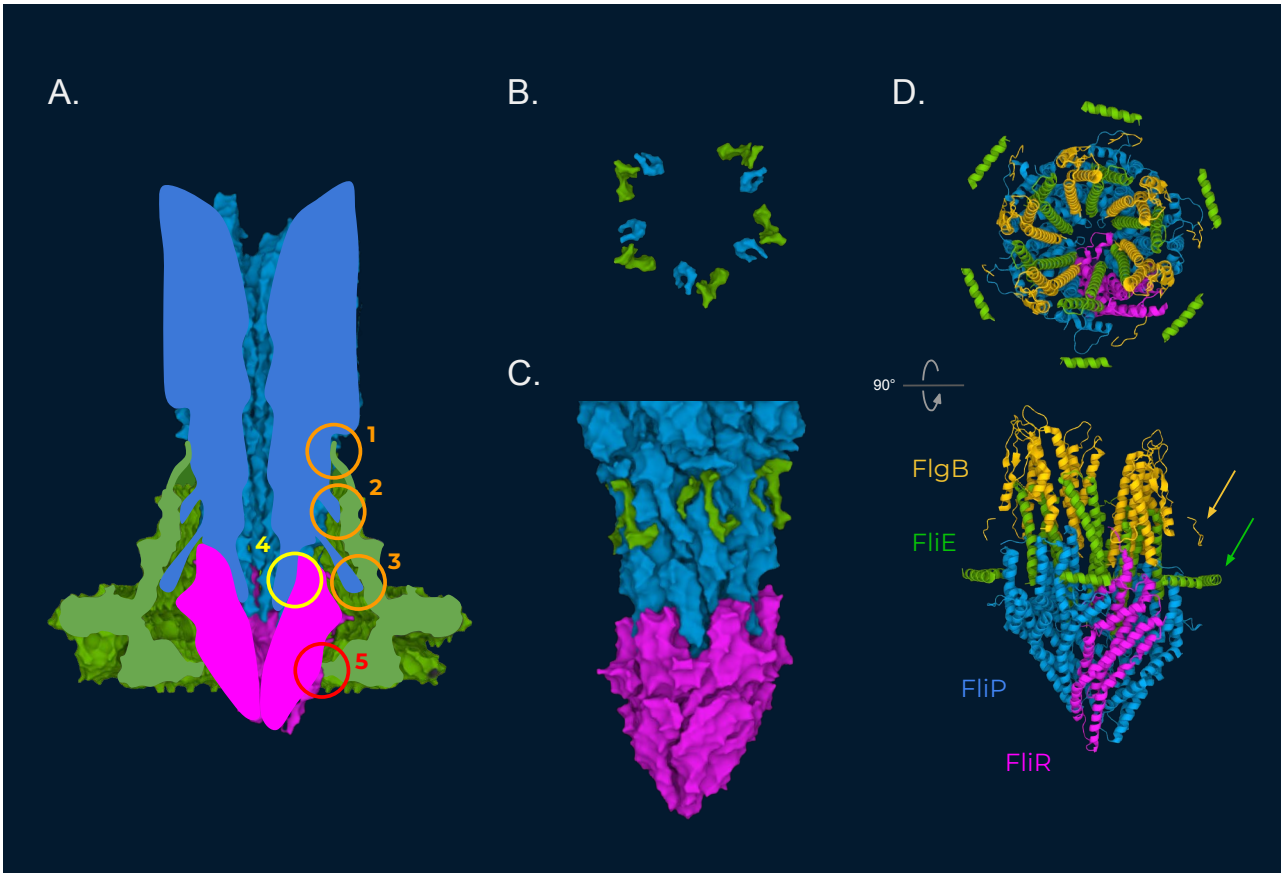

Figure 15. Connections between the driveshaft (rod), export gate and hub (MS-ring). (A) Binding sites between the driveshaft and hub are indicated with orange circles. The binding site between the driveshaft and export gate is indicated with the yellow circle. The binding site between the export gate and hub is indicated with the red circle. The driveshaft is coloured blue, the hub is coloured green and the FliPQR complex of the export gate is coloured purple (B) A top-down view of the portions of FliF which extend from the top of the socket of the hub and bind to the driveshaft (labeled 1 in A). Ascending arms (termed L1) are coloured green while descending arms (termed L2) are coloured blue. (C) The portions of FliF which extend from the top of the socket of the hub are shown in green binding into groves and pockets in the outer surface of the proximal driveshaft, shown in blue (PDB ID: 7E80). The FliPQR complex of the export gate is shown in purple (D) The connection between the driveshaft and export gate, coloured as in figure 13 (FliQ not shown) (PDB ID: 7CGO[i]). The structure of portions of some of the proteins have not been solved. Alpha helices from the driveshaft and export gate slot into groves on the adjacent component. The yellow arrow points to a portion of FlgB which binds to the upper portion of the hub's socket (labeled 2 in A). The green arrow points to the ring of alpha helices from FliE, which bind to the lower portion of the hub's socket (labeled 3 in A). Despite the core of FliE having helical symmetry as part of the driveshaft, this ring of FliE alpha helices has near-perfect rotational symmetry to bind to the inside of the hub socket which has rotational symmetry.

i) Tan, J., Zhang, X., Wang, X., Xu, C., Chang, S., Wu, H., Wang, T., Liang, H., Gao, H., Zhou, Y., and Zhu, Y., Structural basis of assembly and torque transmission of the bacterial flagellar motor, *Cell* **184**:2665–2679, 2021.

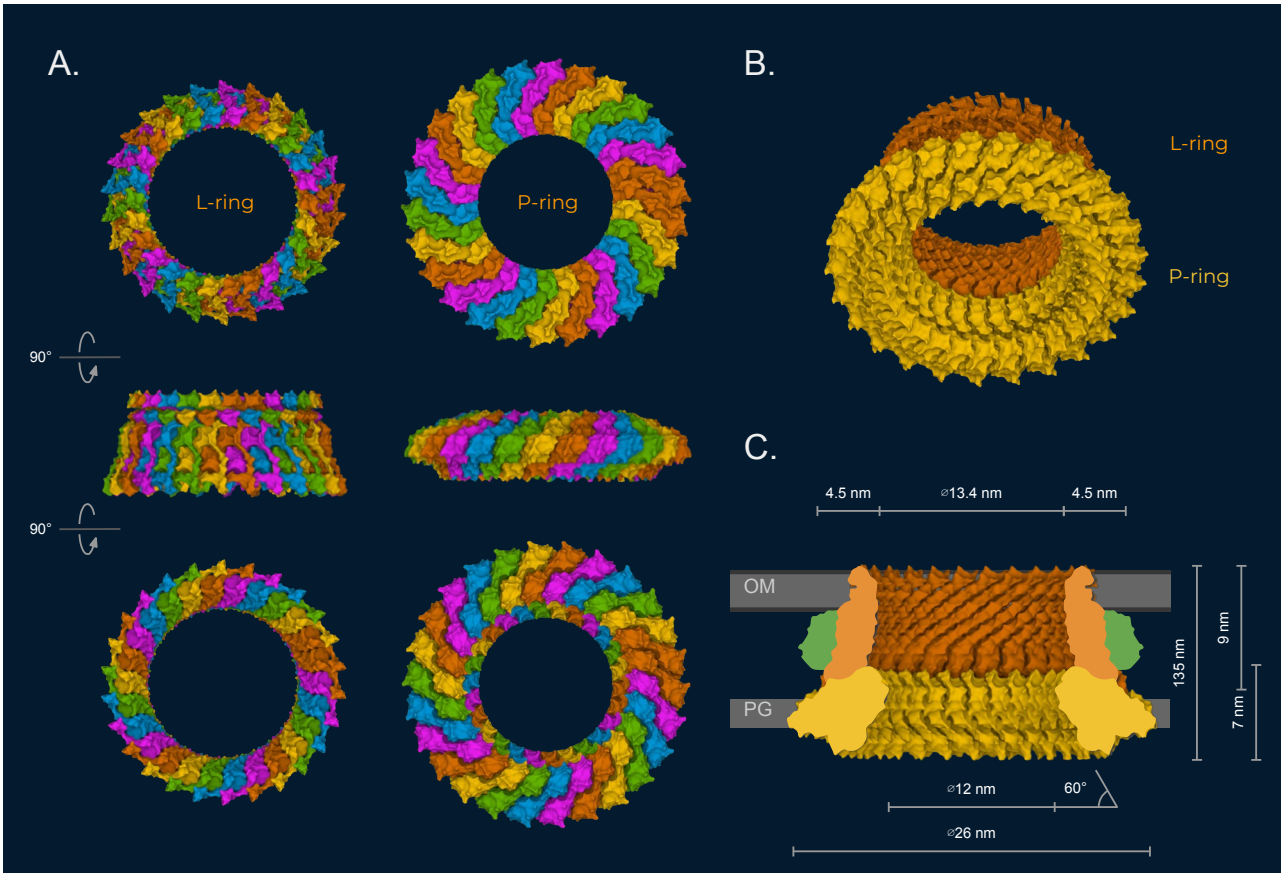

Figure 16. Bushing (L- & P-rings) of *Salmonella* (PDB ID: 7CLR[i]). (A) Molecular surface representation of the L-ring (left) and P-ring (right) showing how the subunits within each ring interlock. (B) 3-dimensional view of the Bushing. The L-ring and P-ring are coloured orange and yellow, respectively. (C) Cross-section diagram of the bushing. The L-ring, P-ring and YecR ring are coloured orange, yellow and green, respectively.

i) Yamaguchi, T., Makuno, F., Miyata. T., Minamino, T., Kato. T., and Namba, K., Structure of the molecular bushing of the bacterial flagellar motor, *Nature Commun.* **12**:4469, 2021.

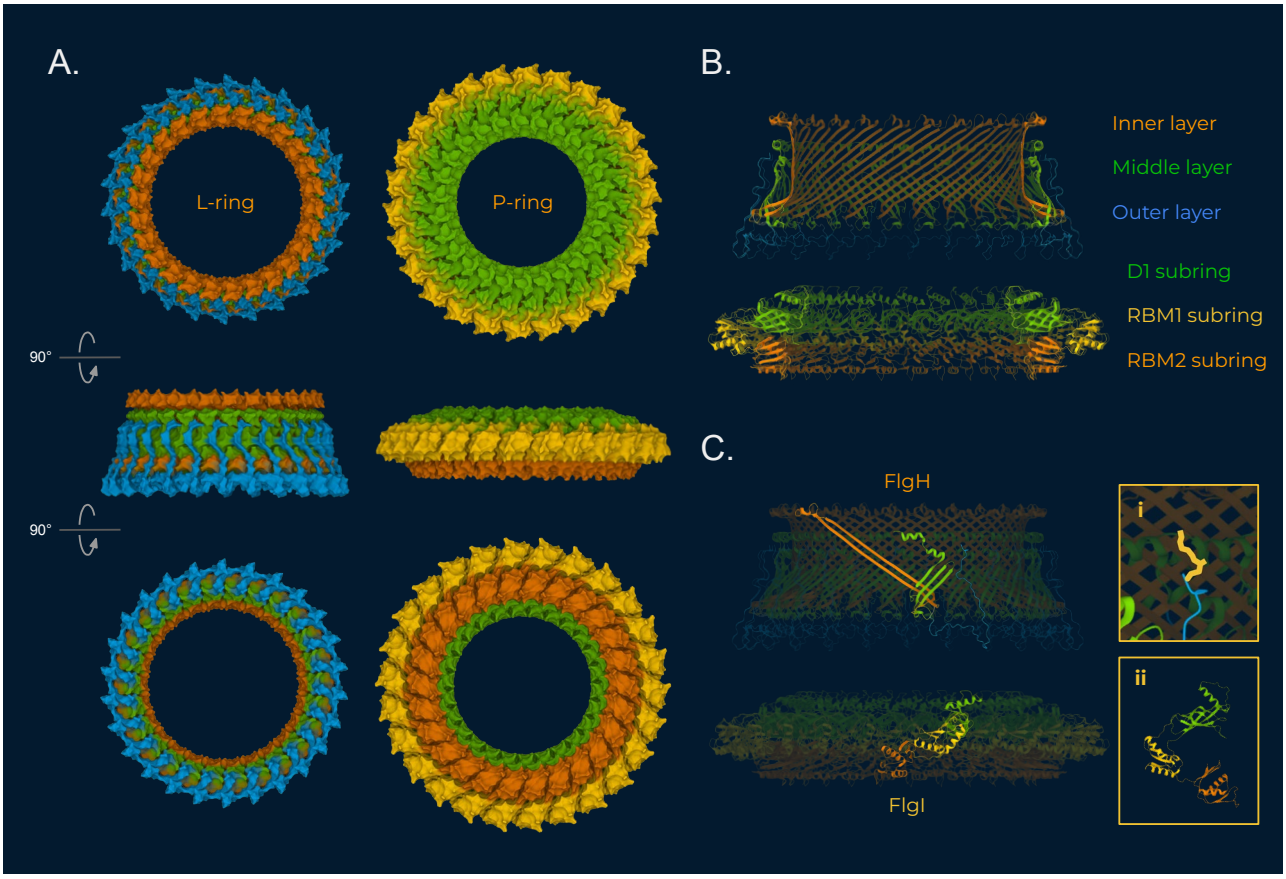

Figure 17. Bushing (L- P-rings) of *Salmonella* (PDB ID: 7CLR). (A) Molecular surface representation of the three layers of the L-ring (left) and the three domain subrings of the P-ring (right). The inner, middle, and outer layers of the L-ring are coloured orange, green and blue, respectively. The D1, RBM1, and RBM2 domains of the P-ring are coloured green, yellow, and orange, respectively. (B) Cross-section of a ribbon diagram representation, coloured the same as in A. The intricate criss-crossing and interweaving of the protein chains can clearly be seen. (C) A ribbon diagram representation of the L-ring (top) and P-ring (bottom) with a single subunit highlighted in front in each ring, coloured the same as in B. Insert (i): Close up of the position of the fatty acetyl group (indicated in yellow) attached to the N-terminal of FlgH (coloured blue). Insert (ii): A different view of the P-ring subunit FlgI, clearly showing the three domains.

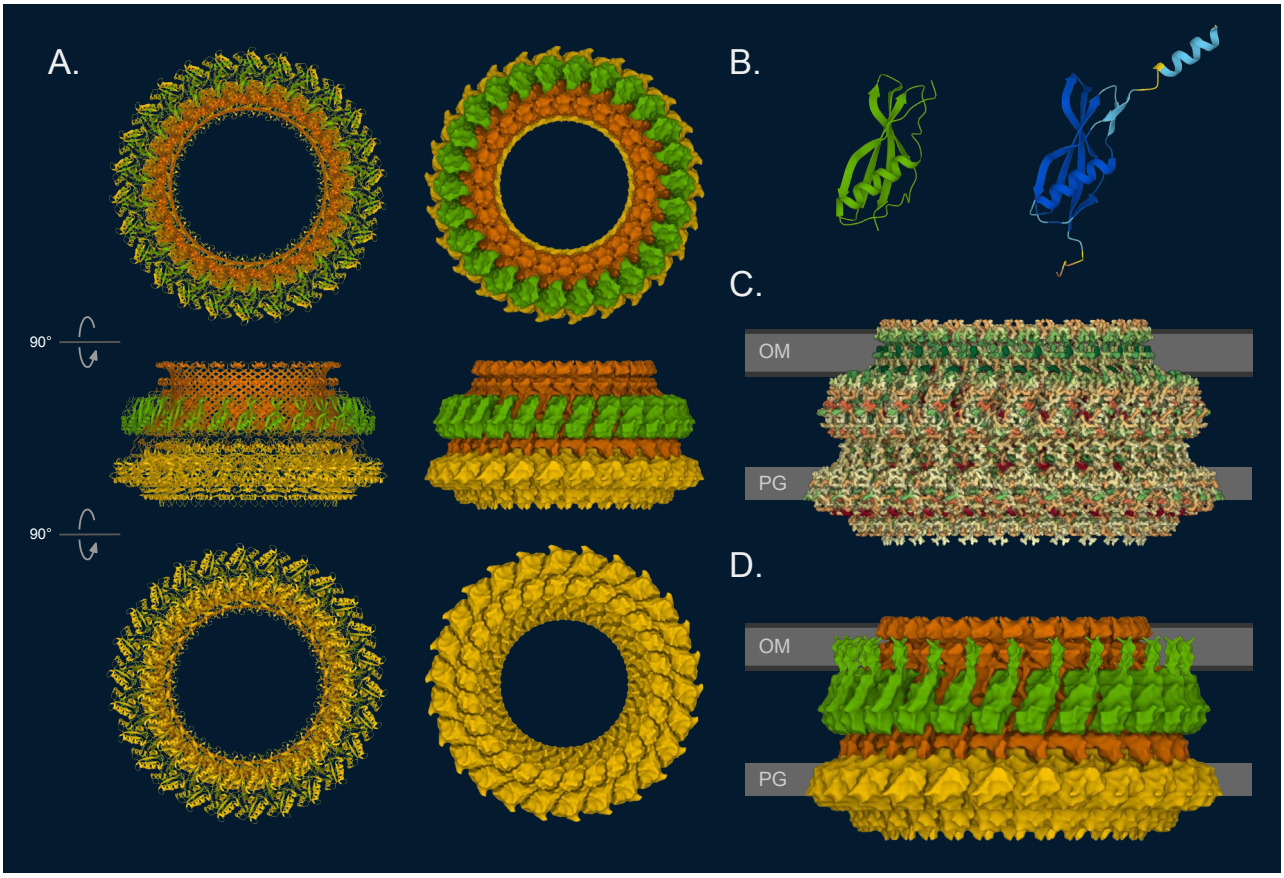

Figure 18. YecR-bushing complex (PDB ID: 7BGL[i]). (A) ribbon diagram representation (left) and molecular surface representation (right) of the YecR-bushing complex. The bottom view of the molecular surface representation clearly shows how perfectly round and smooth the inner hole of the bushing is, in contrast to the outside of the bushing. (B) The solved structure (left, PDB ID:7BGL) and the Alphafold prediction (right, P76308) of YecR. The Alphafold prediction, coloured by prediction confidence, shows the possible structure of the portions of YecR that have not been solved. (C) Hydrophobicity of residues (red= hydrophilic; green = hydrophobic). The approximate position of the hydrophilic and hydrophobic portions of the outer membrane (OM) have been shown in dark gray and light gray, respectively. PG: Peptidoglycan layer. (D) A model of the YecR-bushing complex. The Alphafold prediction of the structure of the membrane-embedded N-terminal of YecR (P76308), which has not been solved experimentally, has been added to the model.

i) Johnson, S., Furlong, E.J., Deme, J.C., Nord, A.L., Caesar, J., Chevance, F., Berry, R.M., Hughes, K.T., and Lea, S.M., Molecular structure of the intact bacterial flagellar basal body, *Nature Microbiol.* **6**:712–721, 2021.

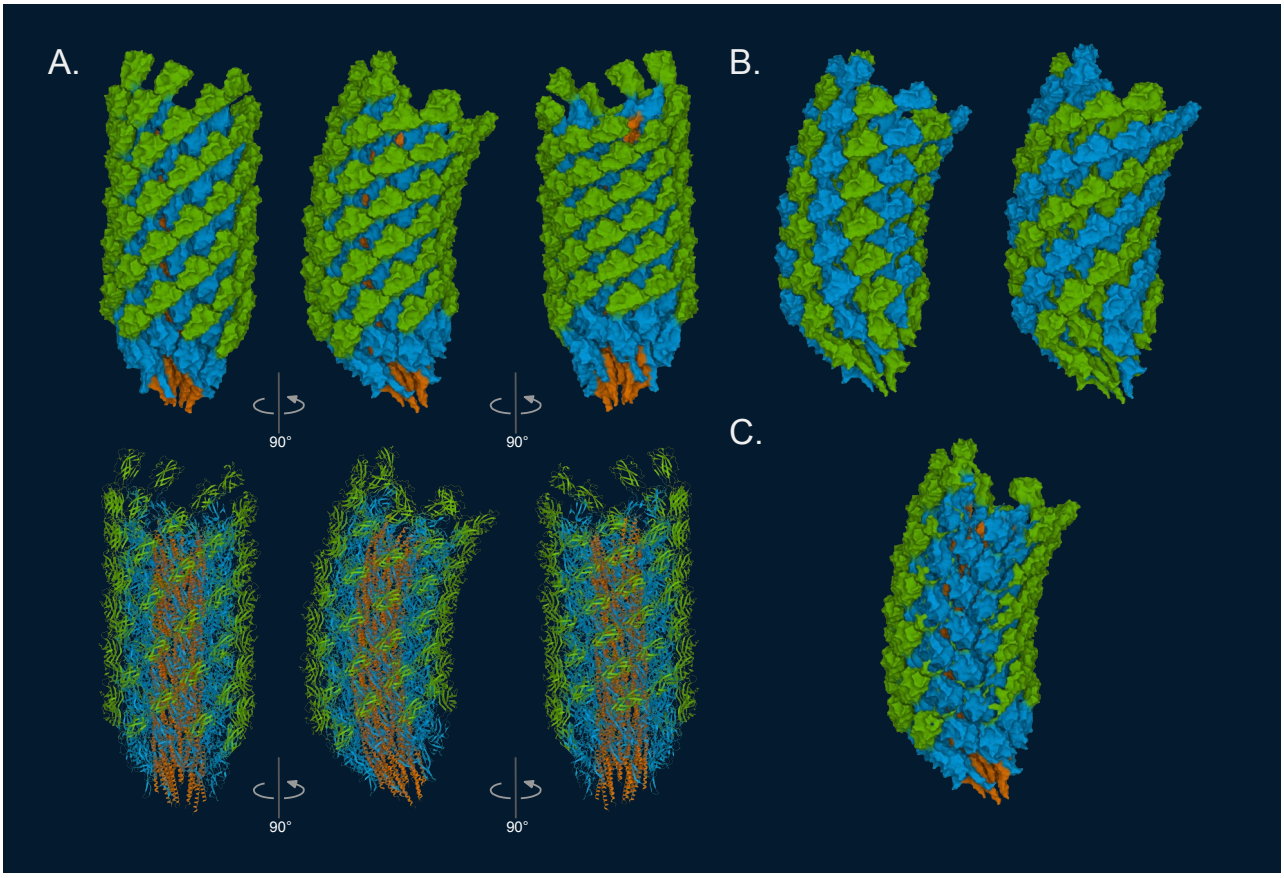

Figure 19. Universal joint (hook) (PDB ID: 6K3I[i]). (A) Molecular surface representation (top) and ribbon diagram (bottom) of 66 subunits of the universal joint. A full-length universal joint contains about 120 subunits. The expanded and contracted arrangement of the outer layer domains (D2), coloured green, are clearly visible. (B) The universal joint with subunits colored blue and green along the 11-start (left) and 6-start (right) helical directions. (C) The model from A. with part of the outer layer shaved off to reveal the mesh-like middle layer.

i) Shibata, S., Matsunami, H., Aizawa, S.I., and Wolf, M., Torque transmission mechanism of the curved bacterial flagellar hook revealed by cryo-EM, *Nature Struct. Mol. Biol.* **26**:941–945, 2019.

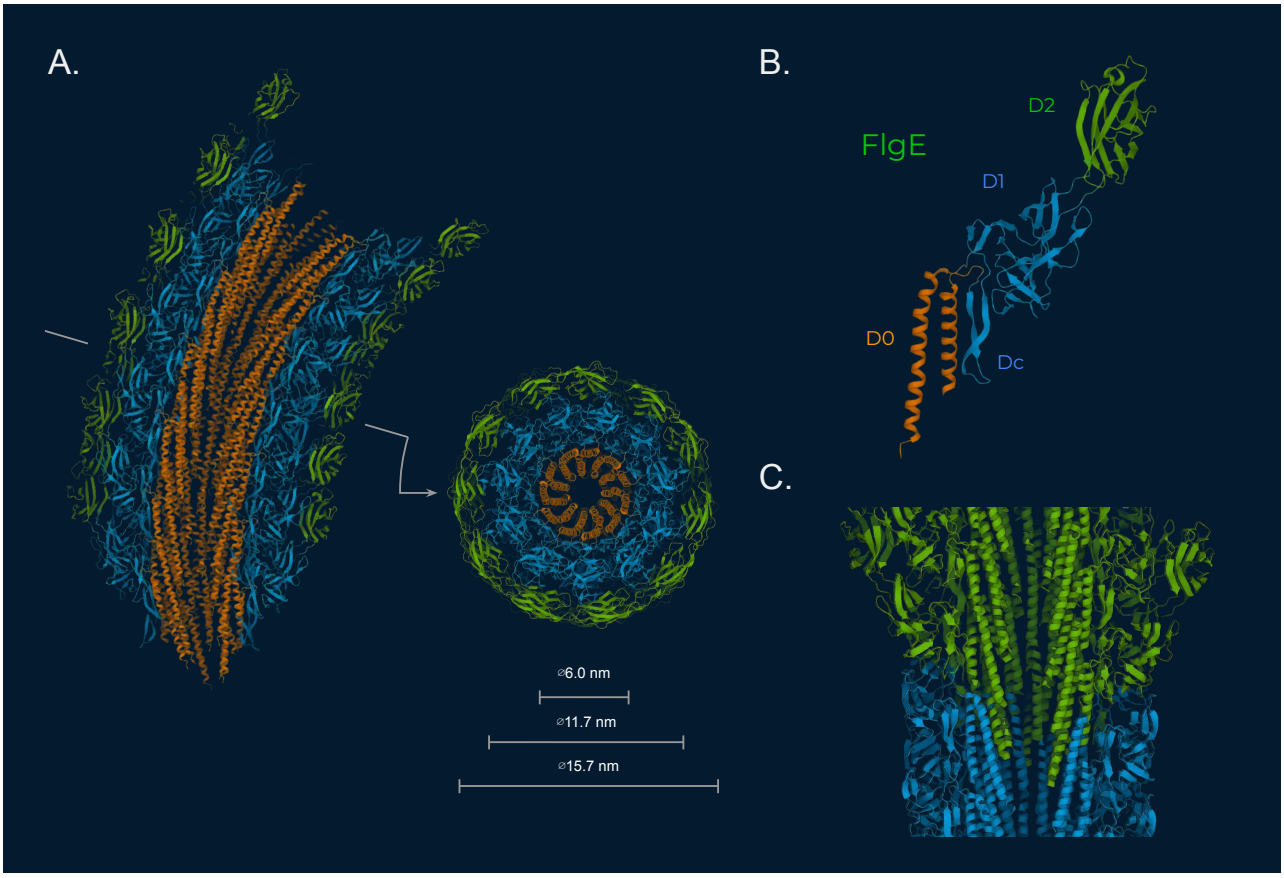

Figure 20. Universal joint (hook). (A) Vertical (left) and horizontal (right) cross-sections through the universal joint (PDB ID: 6K3I). Only about half of the length of the universal joint is shown in the vertical cross-section. (B) ribbon diagram of a single universal joint subunit (FlgE, PDB ID: 6K3I). (C) Vertical cross-section through a ribbon diagram representation of the driveshaft-universal joint connection (PDB ID: 7E80). The driveshaft is shown in blue and the universal joint is shown in green.

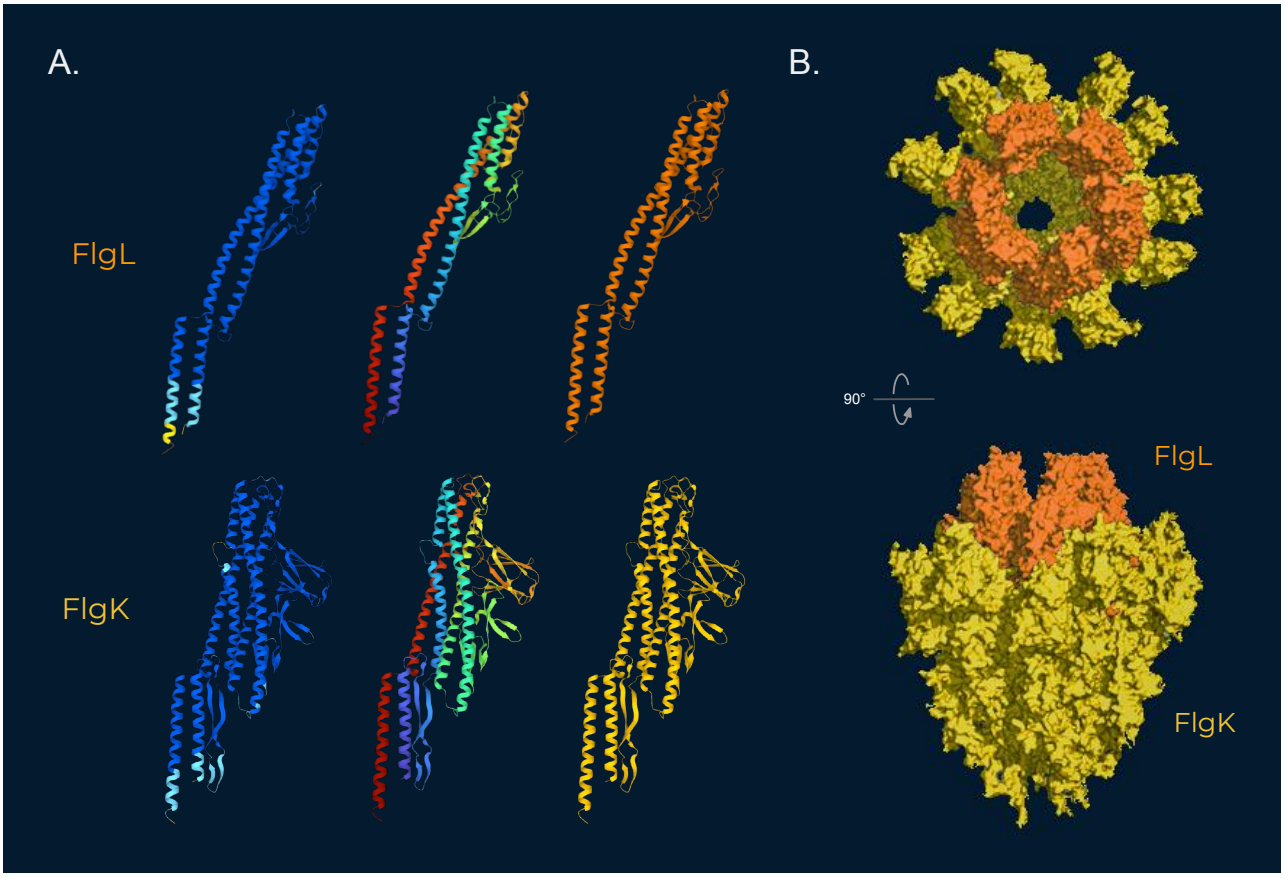

Figure 21. Universal joint-filament junction. (A) Alphafold prediction of FlgL (P29744) and FlgK (P33235) from *E. coli*, colored according to prediction confidence (left), rainbow from the N-terminal to the C-terminal (middle), and uniform colouring (right). (B) Predicted structure of universal joint-filament junction, as predicted by Green A. *et al.*[i] Used with permission. FlgK, which binds to the distal end of the universal joint, is coloured yellow. FlgL, which binds to the proximal end of the filament, is coloured orange.

i) Green, A.G., Elhabashy, H., Brock, K.P., Maddamsetti, R., Kohlbacher, O., and Marks, D.S., Large-scale discovery of protein interactions at residue resolution using co-evolution calculated from genomic sequences, *Nature Commun.* **12**:1396, 2021.

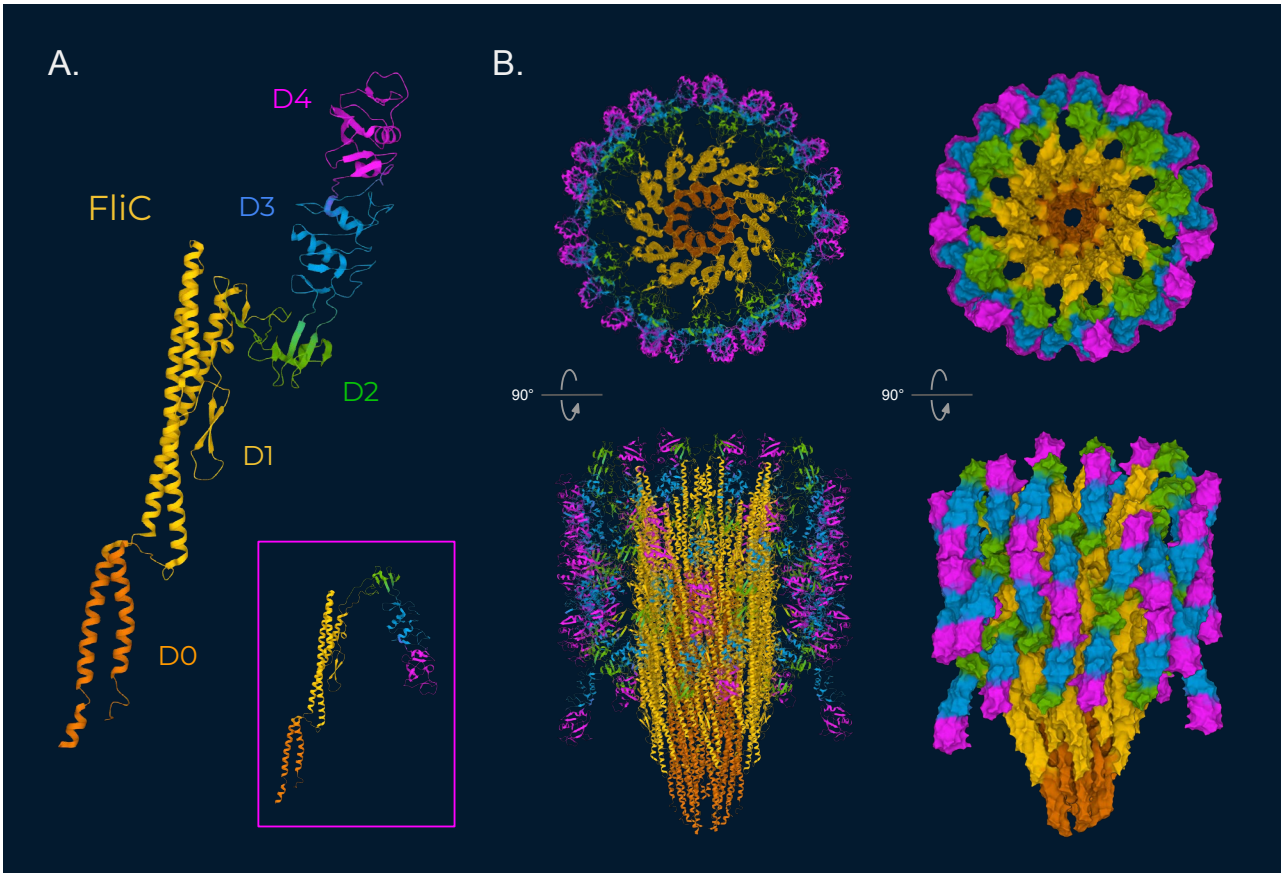

Figure 22. Propeller filament in *E. coli* (O127:H6). (A) Ribbon diagram of FliC from *E. coli* (O127:H6, PDB ID:7SQJ[i]) showing the five domains. Main image is of the outer domains of FliC in an upward orientation. Insert is of the outer domains of FliC in a downward orientation (rotated 180 degrees relative to the upward orientation). There are two slightly different conformations within each of these two outer domain orientations, resulting in four main conformations of FliC present in the filament. The outer domains bind to each other to form tetramers. (B) Ribbon diagram (left) and molecular surface representation (right) of the *E. coli* (O127:H6) filament, colored as in A. This is a composite model made from two copies of the PDB file 7SN7.[i]

i) Kreutzberger, M., Sobe, R.C., Sauder, A.B., Chatterjee, S., Peña, A., Wang, F., Giron, J.A., Kiessling, V., Costa, T., Conticello, V.P., Frankel, G., Kendall, M.M., Scharf, B.E., and Egelman, E.H., Flagellin outer domain dimerization modulates motility in pathogenic and soil bacteria from viscous environments, *Nature Commun.* **13**:1422, 2022.

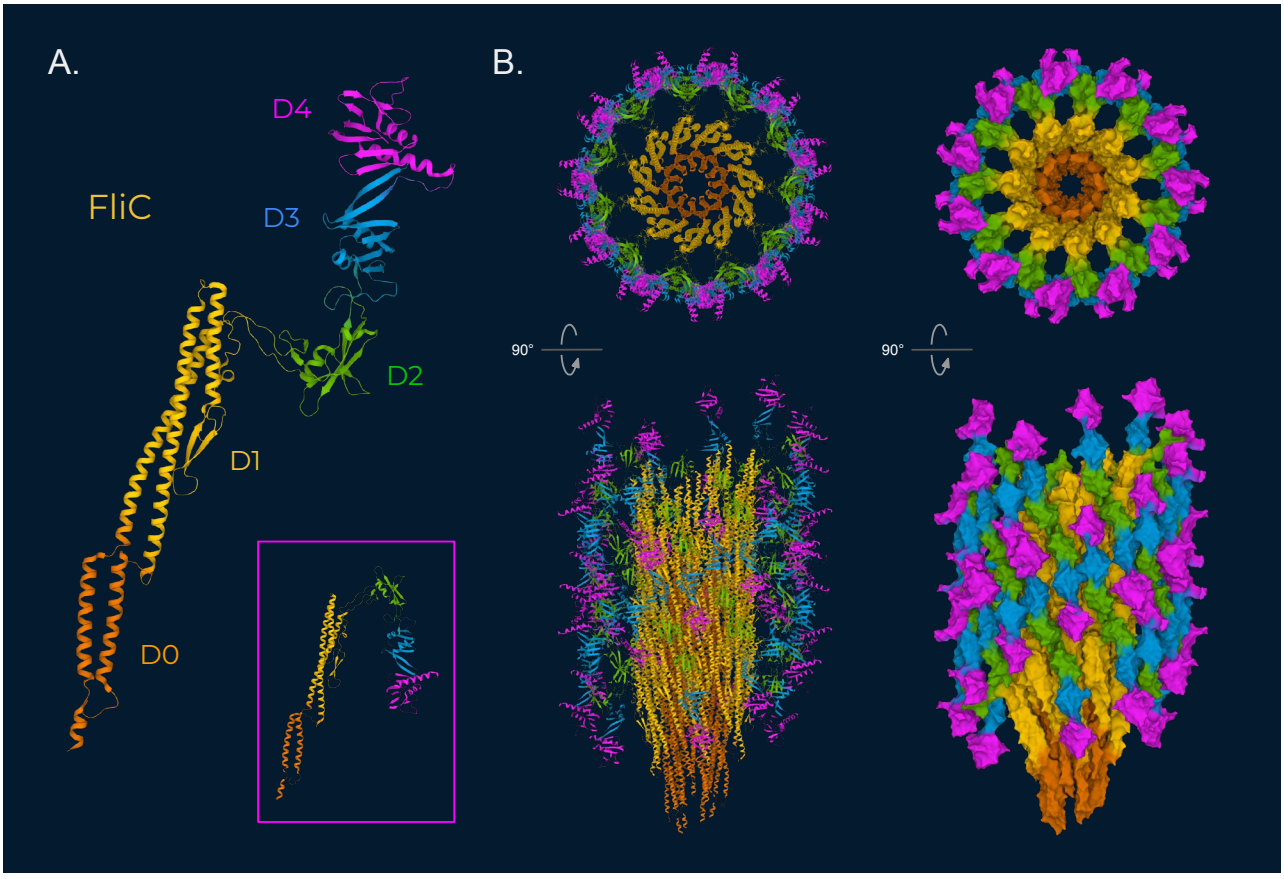

Figure 23. Propeller filament in *E. coli* (O157:H7, PDB ID:7SN4[i]). (A) Ribbon diagram of FliC from *E. coli* (O157:H7) showing the five domains. Main image is of the outer domains of FliC in an upward orientation. Insert is of the outer domains of FliC in a downward orientation (rotated 180 degrees relative to the upward orientation). The outer domains bind to each other to form dimers. (B) Ribbon diagram (left) and molecular surface representation (right) of the *E. coli* (O157:H7) filament (PDB ID:7SN4), colored as in A.

i) Kreutzberger, M., Sobe, R.C., Sauder, A.B., Chatterjee, S., Peña, A., Wang, F., Giron, J.A., Kiessling, V., Costa, T., Conticello, V.P., Frankel, G., Kendall, M.M., Scharf, B.E., and Egelman, E.H., Flagellin outer domain dimerization modulates motility in pathogenic and soil bacteria from viscous environments, *Nature Commun.* **13**:1422, 2022.

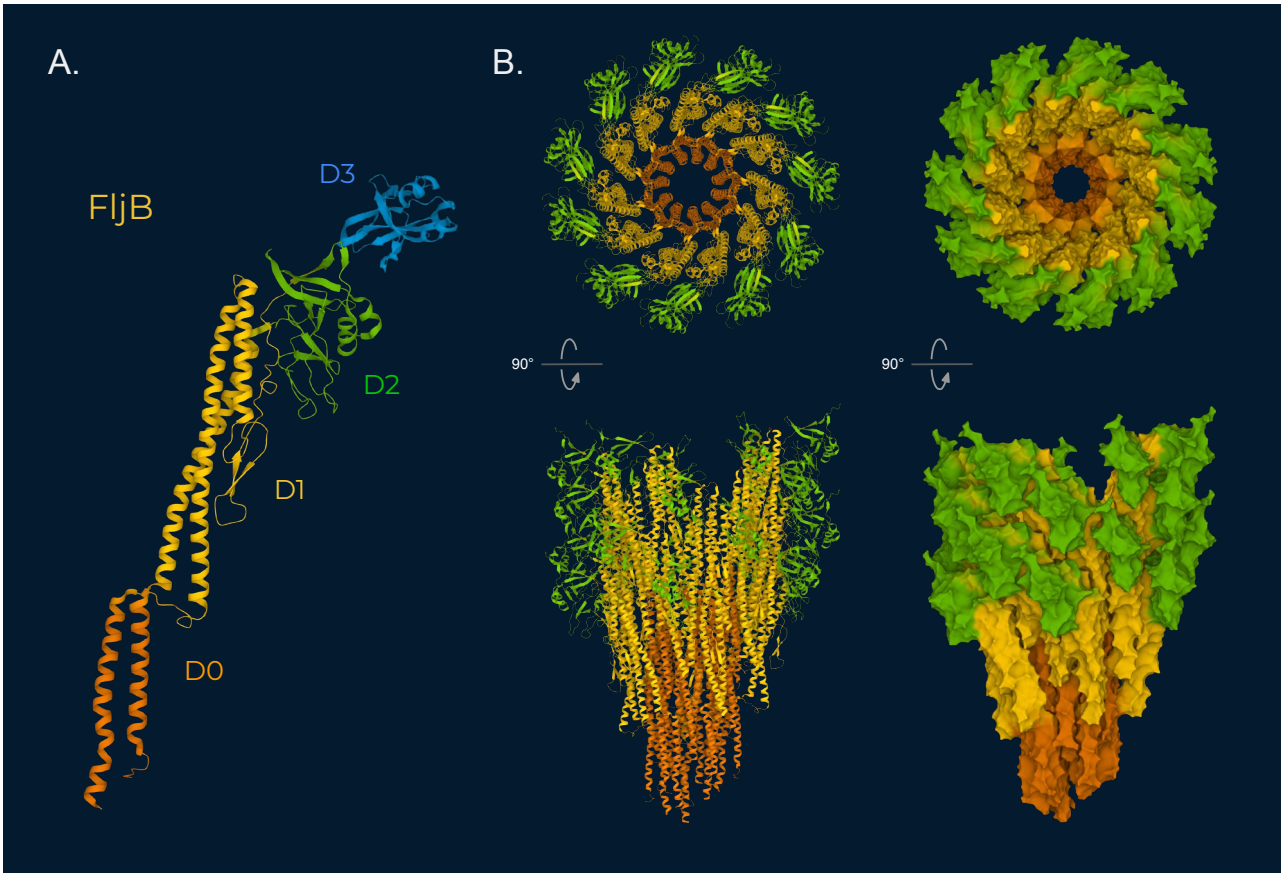

Figure 24. FljB filament from *Salmonella*. (A) Ribbon diagram of FljB from *Salmonella* showing the five domains. Domain D3 is flexible in it's orientation and thus it's structure has not been solved experimentally. Shown here is the Alphafold prediction of D3 (P52616) added to a subunit from PDB file 6JY0. The outer domains to not bind to one another. (B) Ribbon diagram (left) and molecular surface representation (right) of the *Salmonella* FljB filament (PDB ID: 6JY0[i]), colored as in A. (domain D3 not shown).

i) Yamaguchi, T., Toma, S., Terahara, N., Miyata, T., Ashihara, M., Minamino, T., Namba, K., and Kato, T., Structural and functional comparison of salmonella flagellar filaments composed of FljB and FliC, *Biomolecules* **10**(2):246, 2020

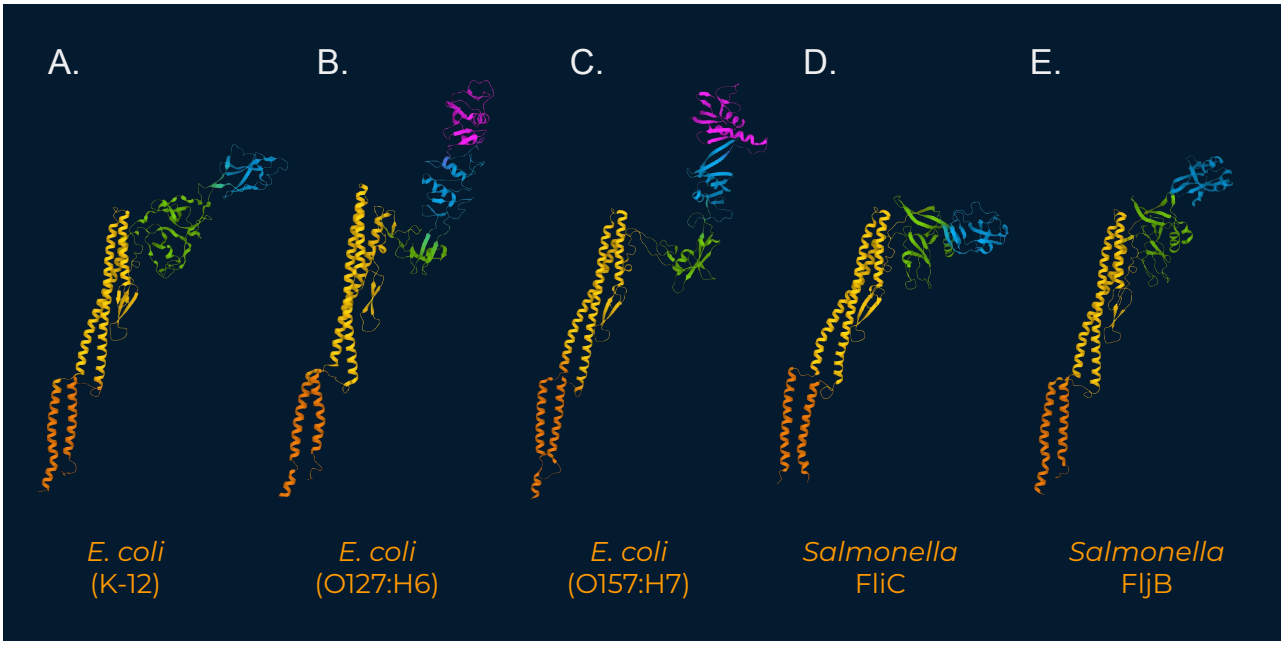

Figure 25. Comparison of flagellin proteins in *E. coli* and *Salmonella*. (A) FliC from *E. coli* K-12 (Alphafold prediction: P04949). (B) FliC from *E. coli* O127:H6 (PDB ID: 7SN7). (C) FliC from *E. coli* O157:H7 (PDB ID: 7SN4). (D) FliC from *Salmonella* (PDB ID: 3A5X). (E) FljB from *Salmonella* (PDB ID: 6JY0 & Alphafold prediction of D3: P52616)

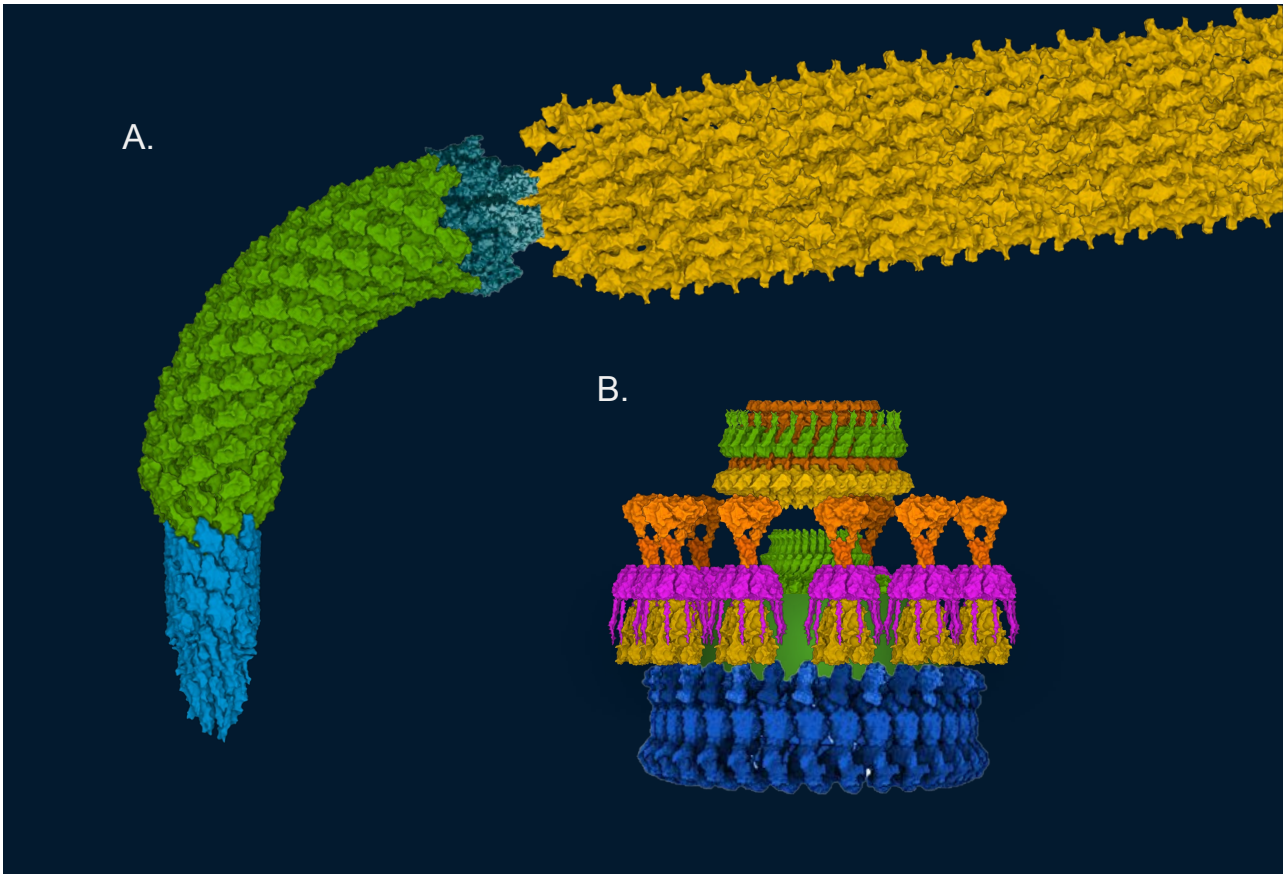

Figure 26. Axial components vs ring components. See the caption of figure 1 for image credit. (A) Axial components: Driveshaft (blue), universal joint (green), universal joint-filament junction (dark blue), and filament (yellow). (B) Ring components, coloured as in Figure 1a. The export apparatus is generally not classified as either an axial or ring component. The export apparatus can be classified as a separate machine which is involved in the construction of the flagellar motor.